Stratospheric Injection of Brominated Very Short-Lived Substances Inferred from Aircraft Observations of Organic Bromine and BrO in the Western Pacific

Pamela A. Wales[1], Ross J. Salawitch[1,2,3], Julie M. Nicely[1,4,5], Daniel C. Anderson[2,6], Timothy P. Canty[2], Sunil Baider[7,8,9], Barbara Dix[7], Theodore K. Koenig[7,8], Rainer Volkamer[7,8], Dexian Chen[10], L. Gregory Huey[10], David J. Tanner[10], Carlos A. Cuevas[11], Rafael P. Fernandez[11,12], Douglas E. Kinnison[13], Jean-Francois Lamarque[13], Alfonso Saiz-Lopez[11], Elliot L. Atlas[14], Samuel R. Hall[13], Maria A. Navarro[14], Laura L. Pan[13], Susan M. Schauffler[13], Meghan Stell[13,15], Simone Tilmes[13], Kirk Ullmann[13], Andrew J. Weinheimer[13], Hideharu Akiyoshi[16], Martyn P. Chipperfield[17], Makoto Deushi[18], Sandip S. Dhomse[17], Wuhu Feng[17], Phoebe Graf[19], Ryan Hossaini[20], Patrick Jöckel[19], Eva Mancini[21], Martin Michou[22], Olaf Morgenstern[23], Luke D. Oman[4], Giovanni Pitari[24], David A. Plummer[25], Laura E. Revell[26,27], Eugene Rozanov[26,28], David Saint-Martin[22], Robyn Schofield[29,30], Andrea Stenke[26], Kane A. Stone[29,30,31], Daniele Visioni[21], Youshuke Yamashita[16,32], and Guang Zeng[23]

[1]Department of Chemistry and Biochemistry, University of Maryland, College Park, Maryland, USA.

[2]Department of Atmospheric and Oceanic Science, University of Maryland, College Park, Maryland, USA.

[3]Earth System Science Interdisciplinary Center, University of Maryland, College Park, Maryland, USA.

[4]Atmospheric Chemistry and Dynamics Laboratory, NASA Goddard Space Flight Center, Greenbelt, Maryland, USA.

[5]Universities Space Research Association, Columbia, Maryland, USA.

[6]Now at: Department of Chemistry, Drexel University, Philadelphia, PA, USA.

[7]Department of Chemistry & Biochemistry, University of Colorado, Boulder, CO, USA.

[8]Cooperative Institute for Research in Environmental Sciences (CIRES), Boulder, CO, USA.

[9]National Oceanic and Atmospheric Administration (NOAA), Boulder, CO, USA.

[10]School of Earth & Atmospheric Sciences, Georgia Tech, Atlanta, Georgia, USA.

[11]Department of Atmospheric Chemistry and Climate, Institute of Physical Chemistry Rocasolano, Spanish National Research Council (CSIC), Madrid, Spain.

[12]Argentine National Research Council (CONICET), FCEN-UNCuyo, UTN-FRM, Mendoza, Argentina.

[13]National Center for Atmospheric Research, Boulder, Colorado, USA.

[14]Department of Atmospheric Sciences, Rosenstiel School of Marine and Atmospheric Science, University of Miami, Miami, Florida, USA.

[15]Metropolitan State University of Denver, Denver, Colorado, USA.

[16]National Institute of Environmental Studies (NIES), Tsukuba, Japan.

[17]School of Earth and Environment, University of Leeds, Leeds, UK.

[18]Meteorological Research Institute (MRI), Tsukuba, Japan.

[19]Deutsches Zentrum für Luft- und Raumfahrt (DLR), Institut für Physik der Atmosphäre, Oberpfaffenhofen, Germany.

[20]Lancaster Environment Centre, Lancaster University, Lancaster, UK.

[21]Department of Physical and Chemical Sciences and Center of Excellence CETEMPS, Università dell'Aquila, 67100 L'Aquila, Italy.

[22]CNRM UMR 3589, Météo-France/CNRS, Toulouse, France.

[23]National Institute of Water and Atmospheric Research (NIWA), Wellington, New Zealand.

[24]Department of Physical and Chemical Sciences, Università dell'Aquila, 67100 L'Aquila, Italy.

[25]Environment and Climate Change Canada, Montréal, Canada.

[26]Institute for Atmospheric and Climate Science, ETH Zürich (ETHZ), Zürich, Switzerland.

[27]Bodeker Scientific, Christchurch, New Zealand.

[28]Physikalisch-Meteorologisches Observatorium Davos World Radiation Centre, Dorfstrasse 33, 7260 Davos Dorf, Switzerland.

[29]School of Earth Sciences, University of Melbourne, Melbourne, Australia.

[30]ARC Centre of Excellence for Climate System Science, Sydney, Australia.

[31]Now at: Massachusetts Institute of Technology (MIT), Boston, Massachusetts, USA.

[32]Now at: Japan Agency for Marine-Earth Science and Technology (JAMSTEC), Yokohama, Japan.

Corresponding author: Pamela A. Wales (pwales@umd.edu)

Key Points:

- Very short-lived bromocarbons, produced by biogenic processes in the tropical oceans, contribute 5 ± 2 ppt to stratospheric bromine
- About 60% of the biogenic bromine enters the stratosphere as organic compounds; the remainder crosses the tropopause as inorganic bromine
- Agreement between modeled and measured stratospheric bromine is greatly improved upon representation of biogenic sources in global models

Abstract

We quantify the stratospheric injection of brominated very short-lived substances (VSLS) based on aircraft observations acquired in the Tropical Western Pacific during the CONvective TRansport of Active Species in the Tropics (CONTRAST) and the Airborne Tropical TRopopause EXperiment (ATTREX) campaigns during winter 2014. The overall contribution of VSLS to stratospheric bromine was determined to be 5**.0** ± 2**.1** ppt, in excellent agreement with the 5 ± 3 ppt estimate provided in the 2014 WMO Ozone Assessment report. Measurements of organic bromine compounds, including VSLS, were analyzed using CFC-11 as a stratospheric tracer. Our analysis indicates that 2.9 ± 0.6 ppt of bromine enters the stratosphere via source gas injection (i.e. organic compounds). A box model, constrained to CONTRAST observations, was used to estimate inorganic bromine (Br_y) from measurements of bromine monoxide (BrO) collected by two instruments. The analysis indicates that 2**.1** ± 2**.1** ppt of bromine enters the stratosphere via product gas injection (i.e. inorganic compounds). We also examine the representation of brominated VSLS within global models that participated in the Chemistry-Climate Model Initiative. The representation of stratospheric Br_y due to VSLS in these models generally lies within the range of our empirical estimate of 5**.0** ± 2**.1** ppt. Models that include an explicit representation of VSLS tend to compare better with observations than models that utilize longer-lived chemicals as a surrogate for VSLS. Nonetheless, the treatment of VSLS in these models provides a significant improvement compared to simulations that neglect this important source of natural bromine to the stratosphere.

1. Introduction

Bromine chemistry plays an important role in the depletion of stratospheric ozone (Wofsy et al., 1975). Historically, the only sources of stratospheric bromine considered in many model calculations of ozone depletion and recovery had been methyl bromide (CH_3Br) and halons (e.g. Douglass et al., 2011). However, numerous studies have indicated that marine biogenic emissions of brominated very short-lived substances (VSLS) constitute an important source of stratospheric bromine (Dorf et al., 2008; Dvortsov et al., 1999; Ko et al., 1997; Pfeilsticker et al., 2000; Salawitch et al., 2005). It has been shown that incorporating VSLS into models improves agreement between simulated and measured trends in column ozone (Feng et al., 2007; Salawitch et al., 2005; Sinnhuber & Meul, 2015) and has a significant effect on projections of the

depth and potentially the timing for the recovery of the Antarctic ozone hole (Fernandez et al., 2017; Oman et al., 2016). Additionally, the inclusion of VSLS alters the modeled sensitivity of the ozone layer to both future volcanic eruptions (Klobas et al., 2017) and geoengineering of climate via injection of stratospheric sulfate (Tilmes et al., 2008, 2012). Finally, accurate calculations of tropospheric bromine monoxide (BrO) loading based on satellite measurements of total column BrO rely on proper representation of the stratospheric injection of brominated VSLS (Choi et al., 2012; Salawitch et al., 2010; Theys et al., 2011).

Very short-lived substances are compounds that have lifetimes of six months or less due to photochemical loss in the global troposphere. Since compounds with lifetimes less than six months cannot be assumed to be well mixed within the troposphere (Ko and Poulet et al., 2003), the stratospheric input of VSLS is more sensitive to the geographic location of atmospheric release than the input of CH_3Br and halons, which have atmospheric lifetimes ranging from 0.8 to 65 years. Thus, emissions of VSLS in regions of active, vigorous convection (such as the Tropical Western Pacific, TWP) have a much larger probability of reaching the tropical tropopause layer (TTL) than compounds released in other areas (e.g. Aschmann et al., 2009; Hossaini et al., 2013; Fernandez et al., 2014).

Here, we use the abbreviation VSLS to refer solely to brominated very short-lived substances. The VSLS relevant to this study (i.e., $CHBr_3$, CH_2Br_2, CH_2BrCl, $CHBr_2Cl$, and $CHBrCl_2$) are produced by phytoplankton or algae in the upper ocean (e.g., Tokarczyk and Moore, 1994; Carpenter and Liss, 2000; Quack and Wallace, 2003). The bromine contained in VSLS can reach the stratosphere either via source gas injection (SGI) or product gas injection (PGI). If the VSLS reach the stratosphere in the original organic form (termed CBr_y), this is considered SGI. Alternatively, if the VSLS are oxidized in the troposphere, the constituent bromine atoms rapidly produce inorganic bromine compounds (termed Br_y) such as: BrO, Br, HBr, HOBr, $BrONO_2$, $BrNO_2$, Br_2, and BrCl. If the Br_y product gases reach the stratosphere, this is termed PGI. Consequently, SGI and PGI are sensitive to the strength of convection relative to the lifetime of the VSLS as well as the partitioning of product gases into soluble compounds that are susceptible to both washout and heterogeneous recycling (Aschmann et al., 2011; Fernandez et al., 2014; Hossaini et al., 2010; Liang et al., 2010, 2014; Schofield et al., 2011; Sinnhuber & Folkins, 2006; Tegtmeier et al., 2012).

Prior estimates of the contribution of VSLS to the stratospheric bromine loading are summarized in the most recent World Meteorological Organization Ozone Assessment (WMO 2014) (Carpenter and Reimann et al., 2014). The total contribution of VSLS to stratospheric bromine (i.e., SGI + PGI, denoted Br_y^{VSLS}) was assessed to be 5 ± 3 parts per trillion by volume (ppt). The best estimate for SGI of VSLS (SGI^{VSLS}) presented in WMO 2014 is 1.4 ppt, with a range of 0.7 to 3.4 ppt, based on measurements of VSLS at the average tropical tropopause height of 17 km (e.g., Schauffler et al., 1999; Laube et al., 2008; Brinckmann et al., 2012). Observations of Br_y compounds at the tropical tropopause are sparse (Dorf et al., 2008; Werner et al., 2017). As a result, PGI has previously been estimated to be 1.1 to 4.3 ppt based on a range of global model simulations of the fate of VSLS released by oceanic emissions (Aschmann & Sinnhuber, 2013; Hossaini et al., 2012; Liang et al., 2010, 2014). The WMO 2014 estimate for PGI is consistent with the abundance of Br_y reported around 17 km in the tropics by Dorf et al. (2008) as well as the range of Br_y mixing ratios at the base of the TTL and above the cold point tropopause reported by Werner et al. (2017). The combined observed SGI^{VSLS} and modeled PGI value generally agrees with estimates of Br_y^{VSLS} that are based on analysis slant column measurements of BrO in the middle to upper stratosphere (e.g. Dorf et al., 2008; Parrella et al., 2013; Schofield et al., 2004). However, there are significant uncertainties concerning the modeled estimates of PGI (e.g. Liang et al., 2014; Sinnhuber & Folkins, 2006; Tegtmeier et al., 2012) as well as the inference of Br_y from measurements of BrO for photochemically aged stratospheric air (Kreycy et al., 2013; Sioris et al., 2006).

In this study we use measurements of organic source gases and BrO, collected in the TTL and lower stratosphere of the TWP, to quantify both SGI^{VSLS} and PGI. The TWP, particularly during boreal winter, is a region of active convection and the most important pathway for compounds with short tropospheric lifetimes to reach the stratosphere (Aschmann et al., 2009; Bergman et al., 2012; Levine et al., 2007; Schofield et al., 2011). Consequently, the TWP and nearby Southeast Asia have been regions of focus for a number of ground and ship-based campaigns to study oceanic emissions of VSLS (Brinckmann et al., 2012; Mohd Nadzir et al., 2014; Robinson et al., 2014). Additionally, aircraft campaigns observed mixing ratios of VSLS in Southeast Asia that were slightly elevated with respect to measurements collected in rest of the tropics (Sala et al., 2014; Wisher et al., 2014). However, past campaigns in the TWP did not sample the TTL or the lower stratosphere. Strong convection and potentially suppressed

158 mixing ratios of OH (Rex et al., 2014) could enable efficient transport of VSLS to the TTL. Due
159 to uncertainties in the removal of product gases (Liang et al., 2014; Sinnhuber & Folkins, 2006;
160 Tegtmeier et al., 2012) as well as transport of source gases within the TTL, direct observations of
161 VSLS and their product gases within air entering the stratosphere is required to better constrain
162 SGI^{VSLS} and PGI.

163 In the winter of 2014, three aircraft campaigns based in Guam (13.5°N, 144.8°E)
164 extensively sampled the TWP, including the TTL and lower stratosphere. Our study is based on
165 analysis of data collected during the NASA ATTREX (Jensen et al., 2017) and the NSF
166 CONTRAST campaigns (Pan et al., 2017). The ATTREX campaign sampled air masses up to 20
167 km, while CONTRAST included measurements up to 15 km. The third campaign, Coordinated
168 Airborne Studies in the Tropics (CAST) (Harris et al., 2017), provided measurements of VSLS
169 (Andrews et al., 2016) and BrO (Le Breton et al., 2017) from the marine boundary layer up to 8
170 km over the TWP. Since our emphasis is on analysis of observations that reach the TTL and
171 cross into stratosphere, data from CAST are not shown.

172 We rely on measurements of CH_3Br, halons, and a suite of organic VSLS provided by the
173 Whole Air Sampler (WAS) instruments (Navarro et al., 2015) during both ATTREX and
174 CONTRAST. We also utilize measurements of BrO obtained by two instruments during
175 CONTRAST: in situ observations from a chemical ionization mass spectrometer (CIMS) (Chen
176 et al., 2016) and remote observations from an Airborne Multi AXis Differential Optical
177 Absorption Spectroscopy (AMAX-DOAS) instrument (Koenig et al., 2017). A limb-scanning
178 mini-differential optical absorption spectroscopy (mini-DOAS) instrument measured BrO during
179 ATTREX (Stutz et al., 2017; Werner et al., 2017). However, at the time of writing, observations
180 of BrO from the mini-DOAS for the winter 2014 phase of ATTREX are not available.

181 Our study builds upon prior analyses of ATTREX and CONTRAST data. Navarro et al.
182 (2015) presented an estimate of SGI^{VSLS} based on WAS observations of organic compounds
183 acquired during ATTREX and PGI based on a model estimate of gas phase Br_y. Both Chen et al.
184 (2016) and Koenig et al. (2017) estimated PGI using observations of BrO at the base of the
185 stratosphere acquired during CONTRAST, but did not incorporate estimates of the
186 decomposition of organic compounds for air parcels within the stratosphere. In this study, we use
187 empirical bromocarbon-tracer relations to combine all three sets of observations (i.e., WAS
188 organics plus CIMS and AMAX-DOAS BrO) to develop comprehensive estimates of SGI^{VSLS},

PGI, and overall Br_y^{VSLS}. Since our study examines measurements obtained within the lower stratosphere and incorporates a method for quantifying the contribution to BrO from the stratospheric decomposition of source gases, our value of PGI is likely more robust than prior estimates because a larger ensemble of air masses is represented. We have made no attempt to quantify the amount of PGI that results from the oxidation of VSLS or other sources, such as sea salt aerosol. We refer the interested reader to Koenig et al. (2017) for analysis concerning the possible contributions of sea salt aerosol as well as stratospheric injection of brominated particles to PGI.

We also compare the combined CONTRAST and ATTREX based estimate of Br_y^{VSLS} to the equivalent representation of this term within 14 global models that participated in the Chemistry-Climate Model Initiative (CCMI) (Morgenstern et al., 2017b). These global models simulate factors that govern tropospheric chemistry, climate change, and ozone depletion. Eyring et al. (2013) recommended that CCMI models incorporate the WMO 2011 best-estimate for Br_y^{VSLS} of 5 ppt (Montzka and Reimann et al., 2011) in one of two manners: either by explicitly including $CHBr_3$ and CH_2Br_2 (the two major VSLS) in the model or by increasing the surface mixing ratio of CH_3Br (a traditional, non-VSLS source of bromine) by 5 ppt relative to baseline, to act as a surrogate for the additional bromine from VSLS. Recent studies have evaluated different emission inventories for VSLS that utilize more detailed emission schemes than recommended for the first phase of CCMI (Hossaini et al., 2013, 2016; Lennartz et al., 2015). Model output from these recent runs are not provided in the public CCMI archive. Our focus is on the analysis of archived CCMI model simulations over long historical (1960 – 2010) and forecast (1960 – 2100) time scales conducted to study the interaction between climate change and atmospheric chemistry (Morgenstern et al., 2017a; Revell et al., 2017).

2. Observation and Model Descriptions

2.1. CONTRAST and ATTREX campaigns

Observations from the CONTRAST and ATTREX campaigns provide a comprehensive suite of chemical and physical measurements of air entering the stratosphere from the TWP. During the CONTRAST campaign, the Gulfstream V (GV) High-performance Instrument Airborne Platform for Environmental Research (HIAPER) payload collected measurements from the marine boundary layer up to 15 km (Pan et al., 2017), and during the ATTREX campaign the

NASA Global Hawk (GH) sampled air masses primarily between 14 and 20 km (Jensen et al., 2017). The Guam-based flights of CONTRAST occurred between 17 January 2014 and 24 February 2014, whereas the Guam-based phase of ATTREX took place between 12 February 2014 and 12 March 2014.

Only two CONTRAST research flights (RF), RF06 (24 January 2014) and RF15 (24 February 2014), reached the stratosphere. Consequently, data collected during RF06 and RF15 are the primary focus of this study. The GV flew north of Guam into the extratropical lowermost stratosphere (LMS) on both flights, as shown in Figure 1. Panels b and c of this figure also include a cross section of potential temperature, the pressure of the thermal tropopause (black dashed lines), as well as the 2 potential vorticity unit (PVU = 10^{-6} K m^{-2} kg^{-1} s^{-1}) surface (green dashed lines), for the respective flight dates. Additionally, zonal winds are shown in Figure S1 to indicate where the GV crosses the subtropical jets. These meteorological fields are from the National Center for Environmental Prediction's final (NCEP-FNL) Operational Global Analysis, which is provided every six hours, at 1°× 1° (latitude, longitude) resolution. The NCEP-FNL data were interpolated bilinearly in latitude and longitude, and linearly in time and pressure, to the GV flight track. Throughout most of this study, the GV is considered to have entered the stratosphere where it crosses the thermal tropopause, as defined by WMO (World Meteorological Organization, 1957). The sensitivity of major results to the tropopause definition is quantified in Section 3.3 by also using the 2 PVU surface (i.e. the dynamical tropopause). Data collected on CONTRAST research flights other than RF06 and RF15 are also used to describe the profile of bromocarbons throughout the TWP troposphere. Tracks of these other flights are shown in Pan et al. (2017).

Measurements from the seven ATTREX flights (transit to Guam, RF01 to RF06) that sampled the stratosphere above the TWP are used. Flight tracks are shown in Figure 2. Here, we only use ATTREX measurements of the nine organic compounds described in Section 2.1.1 that were acquired within the TWP. We define the TWP as between latitudes of 20°S to 20°N and longitudes of 120°E to 165°E. Flight segments within the TWP are shown using blue. Figure 2b shows the GH track along with cross sections of NCEP-FNL meteorological fields for a typical ATTREX flight, RF04, which took place on 6 March 2014. In all flights, the GH provided extensive sampling within the tropical stratosphere by traveling vertically in the tropics to collect

measurements above the tropical tropopause. Conversely, during CONTRAST the GV sampled the extratropical stratosphere by flying horizontally across the subtropical jet (Figure 1).

2.1.1. Aircraft Observations

The University of Miami Whole Air Sampler (WAS) instruments collected measurements of trace gases, including CFC-11 (CF_3Cl) and bromocarbons during both ATTREX and CONTRAST (Andrews et al., 2016; Navarro et al., 2015). During the CONTRAST campaign the WAS configuration is referred to as the Advanced WAS (AWAS), while during the ATTREX campaign the WAS configuration is the GH WAS (GWAS). The WAS instruments collected air samples in canisters that were later analyzed using gas chromatography/mass spectrometry (GC/MS). Differences between inlet and canister systems onboard the two aircrafts are described in Andrews et al. (2016). Both sets of measurements were calibrated using the method described by Schauffler et al. (1999) and analyzed using the same GC/MS system. Our study focuses on WAS measurements of five VSLS ($CHBr_3$, CH_2Br_2, CH_2BrCl, $CHBr_2Cl$, and $CHBrCl_2$), three longer-lived bromocarbons [CH_3Br, halon-1211 ($CBrClF_2$), and halon-2402 ($C_2Br_2F_4$)], and CFC-11. The WAS uncertainty and limit of detection for these nine compounds is given in Table S1 of the supporting information. Overall, measurements and calibrations of VSLS collected by AWAS agrees well with other instruments during CONTRAST and CAST (Andrews et al., 2016).

Halon-1301 ($CBrF_3$) was not measured during CONTRAST and ATTREX by any instrument. Therefore, computed values of halon-1301 as a function of CFC-11 from the CAM-chem-SD global model (described in Section 2.1.2) are used to provide complete representation of all important organic bromine sources. Uncertainty in WAS measurements of these compounds (plus the use of modeled halon-1301 from CAM-chem-SD) are minor factors in the overall uncertainty of our scientific conclusions. Additionally, since halon-1301 is stable within the troposphere, we expect mixing ratios at the base of the stratosphere to be similar to surface observations (Prinn et al., 2000), and there is close agreement between surface WMO measurements and CAM-chem-SD simulations (see Section 3.1.2).

Measurements of CFC-11 acquired by the AWAS instrument aboard the CONTRAST GV are shown in Figure 3, for the segments of RF06 and RF15 that sampled the stratosphere. The dashed vertical lines denote crossings of the thermal tropopause. During RF06, the aircraft sampled stratospheric air only where potential temperature was below 380 K (Figure 1b), which

means air masses could have entered the stratosphere through recent, isentropic transport from the tropical troposphere (Holton et al., 1995). Observed CFC-11 reached a minimum of 227 ppt, only slightly lower than the mean value of 233 ppt observed between 16.5 and 17.5 km in the TWP. During RF15, the aircraft reached air parcels with a potential temperature just above 380 K, indicative of the stratospheric overworld. Minimum CFC-11 was 188 ppt, demonstrating much deeper penetration of the stratosphere and a more photochemically aged chemical composition than sampled during RF06.

While many other chemical and physical measurements acquired by the GV HIAPER payload during RF06 and RF15 are used in our study, the time series central to our analysis are shown in Figure 3. Previous CONTRAST bromine studies (Chen et al., 2016; Koenig et al., 2017) have used the relation between mixing ratios of O_3, CO, and H_2O collected during RF15 to chemically define both the stratosphere as well as a transition layer, where there is a mixture of tropospheric and stratospheric air. While our study primarily uses the thermal tropopause, we also make use of a chemical tropopause (described below) to facilitate comparison to these two studies.

Measurements of O_3, CO, and H_2O are shown in Figure 3. During RF06, chemiluminescence measurements of O_3 (Ridley & Grahek, 1990) peaked at 164 ppb, consistent with the indication that the plane was in the LMS based on potential temperature. For the portion of RF06 where the GV was above the thermal tropopause (between black dashed lines in Figure 3e), observations of CO, provided by an AeroLaser vacuum ultraviolet (VUV) fluorescence instrument (Gerbig et al., 1999), were considerably lower than observed in the troposphere. Conversely, O_3 peaked at 904 ppb on RF15, which was the deepest penetration of the stratosphere for the Guam-based flights of CONTRAST. The extremely low levels of CO observed in the middle portion of RF15 are again consistent with deep penetration of the stratosphere. During both flights, minimum mixing ratios of H_2O (not shown) measured using an open-path laser hygrometer (Zondlo et al., 2010) were around 3 ppm, characteristic of dry stratospheric air.

Koenig et al. (2017) distinguish air for which O_3 is greater than 200 ppb along RF15 as the chemical stratosphere, which provides a comparable view of RF15 to the discussion in Chen et al. (2016). We also use a 200 ppb boundary because this threshold marks a sharp rise in O_3 and a leveling off of the mixing ratios of CO. The two distinct relations between CO and O_3 that

occur on RF15, above and below where O_3 is about 200 ppb, are indicative of the chemically-defined stratosphere and extratropical transition layer (i.e., Pan et al., 2004, 2007; Gettelman et al., 2011).

A key component of our study is the measurement of BrO by two instruments aboard the GV during CONTRAST. The University of Colorado AMAX-DOAS instrument (Baidar et al., 2013; Dix et al., 2016; Volkamer et al., 2015) measured the differential slant column density (dSCD) of BrO and NO_2 horizontally, ahead of the GV. The retrieval of dSCD and the conversion to mixing ratio for BrO and NO_2 are described by Koenig et al. (2017). The AMAX-DOAS measurements of BrO and NO_2 mixing ratios are reported every 30 seconds, as shown in Figure 3 for BrO. Since the AMAX-DOAS instrument measures ahead of the plane, we have applied a 1.8 minute delay is applied to the AMAX-DOAS observations shown in Figure 3g and 3h. Details for the calculation of this delay are given in supporting information (Text S1 and Figure S2). The total measurement uncertainty for BrO and NO_2 is the root sum of squares combination of the dSCD fitting error and the 30% uncertainty in the volume mixing ratio conversion (Dix et al., 2016). The total error for AMAX-DOAS BrO is shown by the green errors bars in Figure 3. Throughout the stratospheric portions of RF06 and RF15, the AMAX-DOAS measurement of BrO is above the 0.4 ppt limit of detection.

The Georgia Institute of Technology CIMS instrument (Huey, 2007; Liao et al., 2011) also measured BrO during CONTRAST, as described by Chen et al. (2016). For RF01 through RF08, the use of a Br_2 calibration gas interfered with these measurements, while for RF09 to RF16, a Cl_2 calibration gas that posed no interference was used. As a result, CIMS observations of BrO were reported for RF15 but not RF06. Additionally, CIMS BrO was not reported where O_3 is greater than 480 ppb, due to possible instrumental interferences. Our study uses CIMS 1 minute measurements of BrO acquired during RF15, which have a 1σ total measurement uncertainty of 11.5% (blue points with error bars, Figure 3h). For stratospheric air masses where O_3 is below 200 ppb, CIMS BrO was frequently near or below the 0.6 ppt limit of detection (Chen et al., 2016). The CIMS instrument also reported a measurement of HOBr + Br_2, but we do not consider the observation of HOBr + Br_2 in our estimates of PGI, because data for this quantity are not available where O_3 mixing ratios are above 200 ppb.

The measurements of BrO from AMAX-DOAS exhibit a broad peak value of about 1 ppt for RF06 (Figure 3g). Measurements of BrO from AMAX-DOAS and CIMS peak around 3.5 ppt

and 4.5 ppt, respectively, for RF15 (Figure 3h). The largest consistent offsets between the two observations of BrO for RF15 occurs on the approach and exit from the stratosphere (i.e., in the upper troposphere) and in the region of the lowermost stratosphere where O_3 is below 200 ppb.

2.1.2. CAM-chem-SD

Simulations of the Community Atmosphere Model version 4 with interactive chemistry and specified dynamics (CAM-chem-SD) (Tilmes et al., 2015) were prepared in support of the CONTRAST (Pan et al., 2017) and ATTREX (Jensen et al., 2017) campaigns. Dynamics were specified based on meteorological fields from the NASA Goddard Earth Observing System Model, version 5 (GEOS-5) (Molod et al., 2012). Model output was prepared on a 0.94° latitude by 1.25° longitude resolution with 56 vertical levels and a 30 s temporal resolution. CAM-chem-SD simulations have been used for flight planning of both campaigns as well as post-mission data analysis (Anderson et al., 2016; Koenig et al., 2017; Navarro et al., 2015, 2017; Nicely et al., 2016).

We use output from CAM-chem-SD from a simulation that includes a detailed representation of the chemistry of bromine (Fernandez et al., 2014) and iodine (Saiz-Lopez et al., 2014) compounds, including VSLS and longer-lived bromine sources. All five brominated VSLS measured by the WAS instruments were included in the model. Marine emissions were prescribed based on a parameterization involving satellite measurements of chlorophyll-*a* (Ordóñez et al., 2012). Additional sources of inorganic bromine and chlorine through sea-salt dehalogenation as well as heterogeneous recycling reactions occurring on upper tropospheric aerosols were also considered (Fernandez et al., 2014).

Figure 3 includes time series of BrO found using CAM-chem-SD, interpolated in time and location to the GV flight tracks during CONTRAST RF06 and RF15. The BrO mixing ratios from CAM-chem-SD exhibit close agreement with the AMAX-DOAS retrieval where the GV is above the thermal tropopause during RF06 and within the chemical stratosphere (O_3 > 200 ppb) during RF15. The agreement with CIMS BrO for the chemical stratosphere portion of RF15 is also very good, although there is more variability in the CIMS measurement of BrO than the AMAX-DOAS data. Sharp gradients within the chemical stratosphere are also present in the in situ measurements of O_3 and CFC-11 (Figure 3d). Since AMAX-DOAS is a remote sensing instrument that measures ahead as well as in a narrow band vertically above and below the aircraft, it is possible that AMAX-DOAS observations are not able to capture the gradients in

BrO observed by CIMS. However, the AMAX-DOAS observations of NO_2 do reflect the sharp gradients indicated by observations of O_3 (Figure S2), and the CIMS measurements have known interferences at high mixing ratios of O_3 (Chen et al., 2016). As a result, in lieu of a third observation of BrO, we use measurements from both instruments in a statistical fashion to arrive at a best estimate for Br_y^{VSLS} and PGI.

Furthermore, for the region of the LMS where O_3 < 200 ppb, the mixing ratio of BrO from CAM-chem-SD falls between the AMAX-DOAS and CIMS observations. Within this region, the CIMS observations are close or below the 0.6 ppt lower limit of detection, causing significant variability in the measurements of BrO. Additionally, Koenig et al. (2017) discuss potential reasons for the BrO difference between CAM-chem-SD and AMAX-DOAS where O_3 < 200 ppb, including uncertainties in heterogeneous reaction chemistry and an additional source of Br_y from sea salt aerosols. Difference in the two observations of BrO for this region of the LMS as well as possible shortcomings in modeled BrO supports our use of both measurements of BrO for our baseline determination of Br_y^{VSLS} and PGI.

2.2. Box Model

A photochemical steady-state box model (Choi et al., 2012; Salawitch et al., 2005, 2010; Sioris et al., 2006) was used to infer gas phase Br_y from observed BrO during RF06 and RF15. The box model includes 37 chemical species and uses rate constants and absorption cross sections from the NASA Jet Propulsion Laboratory 2015 (JPL 2015) kinetics compendium (Burkholder et al., 2015) for a complete set of gas phase and heterogeneous chemical reactions known to affect stratospheric BrO. Photolysis frequencies and rate constants were calculated at the location of each AMAX-DOAS and CIMS measurement of BrO for a full diel cycle (at the latitude and pressure of the observation) in 15 minute intervals. The partitioning of all species within the Br_y family was found assuming photochemical steady state over the diel cycle. The modeled BrO/Br_y ratio for the local solar time of each measurement of BrO was then used to infer Br_y along the tracks of RF06 and RF15. Our analysis of Br_y inferred from BrO is restricted to measurements obtained in the stratosphere, as defined by either the thermal or dynamical tropopause.

The box model was constrained to a wide range of GV HIAPER observations, listed in Table 1. One minute averages of GV HIAPER measurements of temperature, pressure, O_3, CO, CH_4, and H_2O were used to constrain the box model. Additionally, surface reflectivity in the

model was scaled so that the modeled photolysis frequency of NO_2 (J_{NO_2}) matched the observation of J_{NO_2} from the HARP instrument. Similarly, total column O_3 was scaled to force agreement between modeled and measured photolysis frequency of O_3, producing $O(^1D)$, $J_{O_3 \rightarrow O(^1D)}$. All other J-values were calculated using these HARP-based estimates of surface reflectivity and total column O_3. The number distribution of particles with diameters between 0.06 and 1 μm was measured using an Ultra-High Sensitivity Aerosol Spectrometer (UHSAS) (Cai et al., 2008). Aerosol surface area density (SAD) was calculated from UHSAS measurements assuming spherical sulfate particles. Due to variability in the aerosol SAD calculated from UHSAS measurements, the box model was constrained to the five-minute running mean of aerosol SAD (Figure S3). We treat all aerosols as sulfate, since the temperature was well above the frost point during all stratospheric observations. We have also specified inorganic chlorine (Cl_y) along the GV tracks of RF06 and RF15 using AWAS measurements of CFC-11, tied to the relation between CFC-11 and Cl_y computed within CAM-chem-SD for the latitudes and longitudes of both flights (Figure S4). Based on our analysis, presented in Section 3.2, this estimate introduces only a minor uncertainty in inferred Br_y.

Chemiluminescence measurements of both NO and NO_2 were acquired during CONTRAST. However, this measurement of NO_2 is believed to have been influenced by an unknown amount of thermally decomposed nitrogen compounds, which leads to an overestimate in the upper troposphere and stratosphere due to the cold conditions of ambient air. Since the modeled BrO/Br_y ratio is sensitive to the trimolecular reaction between BrO and NO_2 (see Section 3.2), total nitrogen oxides (NO_y) in the box model have been scaled to match the mixing ratio of NO_2 reported by the AMAX-DOAS instrument. However, the use of chemiluminescence NO rather than AMAX-DOAS NO_2 as a model constraint indicates a lower abundance of NO_2 (blue line in Figure S2), thereby lowering the amount of Br_y inferred from the observed BrO. As a result, we examine uncertainty in modeled Br_y by also constraining the model to the observed mixing ratio of NO, since the chemiluminescence measurement of NO is unaffected by thermally labile nitrogen compounds due to the design of the instrument. Because NO_2 provides a more direct constraint for the BrO/Br_y ratio, we use AMAX-DOAS NO_2 in our baseline simulations.

The value of Br_y consistent with each observation of BrO along RF06 and RF15 was found in an iterative fashion. The box model was initialized with Br_y from CAM-chem-SD. Box-modeled Br_y was then adjusted so that box-modeled BrO matched either AMAX-DOAS or

CIMS BrO, to within 2%. Analysis of Br_y found in this manner is limited to the stratosphere (i.e., region between the black vertical dashed lines of Figure 3). The effect on computed Br_y of kinetic and measurement uncertainties are considered in Section 3.2 by respectively applying a 1σ displacement in the JPL 2015 uncertainty for the rates of the eight most important chemical reactions that govern the BrO/Br_y ratio and by adjusting model inputs according to their 1σ uncertainty (Table S2).

3. Results and Discussion

3.1. Organic Bromine

3.1.1. Organic Bromine Tracer Relations

Stratospheric tracer-tracer relations were developed using simultaneous WAS measurements of bromocarbons and CFC-11. The use of a stratospheric tracer, such as CFC-11, allows bromocarbons to be analyzed as a function of photochemical aging in the stratosphere (Wamsley et al., 1998) and provides a convenient means for comparing field measurements with the output of global models (e.g. Salawitch et al., 2005, 2010; Kovalenko et al., 2007). Our study uses measurements of CFC-11 and eight bromocarbons to estimate how much Br_y should have formed as a result of the stratospheric decay of both VSLS and longer-lived bromocarbons.

Our procedure for calculating the tracer-tracer relations follows Wamsley et al. (1998). The decay of a long-lived bromocarbon, denoted as (X), in relation to decay of CFC-11 can be represented as:

$$(X) = (X)_o \left[\frac{(CFC\text{-}11)}{(CFC\text{-}11)_o}\right]^{\frac{1}{d}} \quad (1)$$

where $(X)_o$ and $(CFC\text{-}11)_o$ represent the tropical tropopause mixing ratios. For long-lived compounds, such as halons, the decay parameter d in equation (1) is equal to the ratio of the lifetimes (τ) of the bromocarbon relative to CFC-11 (i.e. $d = \tau_X/\tau_{CFC\text{-}11}$) (Plumb & Ko, 1992). However, discrepancies between the observed decay parameter d and the ratio of the lifetimes has been observed for shorter-lived compounds, including CH_3Br (Avallone & Prather, 1997; SPARC, 2013).

Table 2 contains fitting parameters used to define tracer-tracer relations central to our analysis. For our primary analysis of aircraft data, we have taken the logarithm of equation (1), which leads to:

$$\ln(X) = \frac{1}{d}\ln\left[\frac{(\text{CFC-11})}{(\text{CFC-11})_o}\right] + \ln(X)_o \quad (2)$$

and solved for d and $(X)_o$ using linear least-squares analysis of simultaneous measurements of each bromocarbon and CFC-11. The value for $(CFC\text{-}11)_o$ was set to 233 ppt throughout our study, based on the mean of all ATTREX observations of CFC-11 obtained at 17 km altitude (i.e. between 16.5 and 17.5 km) by the GWAS instrument in the TWP. The use of data collected at 17 km to define the abundance of CFC-11 at the base of the stratosphere is also consistent with the approach used in WMO 2014 (Carpenter and Reimann et al., 2014) and other estimates of SGI (i.e., Navarro et al., 2015) because the cold-point tropopause, used to denote the top of the TTL, lies close to 17 km in the tropics. Since many of the bromocarbon compounds have short tropospheric lifetimes, resulting in large seasonal and geographic gradients, solving for $(X)_o$ using equation (2) is more representative of entry into the global stratosphere than values of $(X)_o$ based on ATTREX measurements in the TWP. Comparison of $(X)_o$ from these two methods is given in Section 3.1.2. For Table 2 and throughout, we report values of $(X)_o$ as the mixing ratio multiplied by the bromine atomicity in each compound, since the sum of bromine atoms is used to define SGI. The lifetime of each VSLS at 10 km altitude in the tropics, from Table 1-5 of WMO 2014, is also given for each VSLS.

The relations between the two major VSLS (CH_2Br_2 and $CHBr_3$) and CFC-11, observed during CONTRAST and ATTREX, are shown in Figure 4. Similar plots for the minor VSLS (CH_2BrCl, $CHBr_2Cl$, and $CHBrCl_2$) are shown in supplemental Figure S5, and all fitting parameters calculated using ATTREX observations are given in Table S3. The top panels of Figure 4 show data collected in the extratropical stratosphere during RF06 and RF15 of CONTRAST, whereas the bottom panels show observations in the tropical stratosphere during ATTREX. In all cases, data are shown only if the airplane was in the stratosphere, as defined by the thermal tropopause (Section 2.1.1).

The solid lines in Figure 4 show the fit to the respective data using equation (1). The black points show the values of $(X)_o$ for the various compounds, along with the 1σ fitting uncertainty (numerical values in Table 2). Observations of CH_2Br_2 and $CHBr_3$ versus CFC-11 during ATTREX in the tropical stratosphere (Figures 4c and 4d) can be represented well using equation (1). The same is true for CONTRAST observations of CH_2Br_2 versus CFC-11 in the extratropical stratosphere (Figure 4a). Conversely, CONTRAST observations of $CHBr_3$ versus

CFC-11 exhibit considerable scatter, and are not amenable to being fit using equation (2). The tropical tropospheric lifetimes for CH_2Br_2 and $CHBr_3$, respectively 150 and 17 days (Table 2), provide a likely explanation for this situation.

Compact relations will exist only if the photochemical removal lifetime is long relative to the time scale of mixing (Plumb & Ko, 1992). The ATTREX observations were obtained in a region of the tropical stratosphere characterized by slow ascent ($\theta > 385$ K) and likely isolated from other chemical regimes (e.g., Volk et al., 1996). The CONTRAST measurements, on the other hand, were acquired in the extratropical LMS at potential temperatures between 360 and 385 K, a region that allows for the possibility of rapid horizontal mixing of air parcels with different chemical histories, resulting in a wide range of possible transit times. As discussed above, the decay parameters for CH_3Br and shorter lived compounds will not be a direct function of their lifetime (Avallone & Prather, 1997; SPARC, 2013). For CH_3Br and the two VSLS with longer lifetimes (CH_2Br_2 and CH_2BrCl), the observed decline relative to CFC-11 in the extratropical stratosphere can be adequately described using equation (1). As expected, these compounds exhibit more scatter versus CFC-11 than observed for longer-lived halons (Figure S6). Since the three shortest-lived VSLS ($CHBr_3$, $CHBr_2Cl$, and $CHBrCl_2$) are more sensitive to local chemical environments, meaningful fits could not be determined for CONTRAST observations of these VSLS in the LMS (Figure 4b and Figure S5).

Consequently, Table 2 contains entries for fitting parameters of five VSLS, from a mixture of CONTRAST and ATTREX observations. Together, minor VSLS supply 0.6 ppt to the stratosphere in comparison to $CHBr_3$ and CH_2Br_2, which supply a combined 2.4 ppt. Careful consideration for $CHBrCl_2$ was necessary, because WAS observations were sparse at low mixing ratios of CFC-11 during both CONTRAST and ATTREX. For this species, we used the mean value of $CHBrCl_2$ observed at 17 km (i.e., between 16.5 and 17.5 km) in the TWP during ATTREX to define $(X)_o$. Since the lifetime of $CHBrCl_2$ is closest to the lifetime of $CHBr_2Cl$, the decay parameter from the $CHBr_2Cl$ fit was used.

Finally, Table 2 also shows fitting parameters for the four long-lived bromocarbons (Figure S6) that have traditionally been considered in studies of stratospheric ozone depletion and recovery. For reference, Table 2 also lists the stratospheric lifetimes of these compounds, obtained from Table 1-3 of WMO 2014, originally reported in SPARC (2013). Data acquired in the stratosphere on CONTRAST RF06 and RF15 are used, except for halon-1301, which was not

measured during either CONTRAST, ATTREX, or CAST. The fit parameters for halon-1301 are based on analysis of output from CAM-chem-SD along RF06 and RF15 of CONTRAST. The fits conform to prior expectation (Wamsley et al., 1998) and yield a value of 15.0 ± 0.2 ppt for the sum of the four values of $(X)_o$, which means 15.0 ppt of bromine was delivered to the stratosphere by long lived sources in winter 2014. This estimate is in agreement with the WMO 2014 time series for the delivery of bromine to the stratosphere by these four compounds (Figure S7). Finally, the product of the decay parameter for the various halons and the WMO 2014 estimate of 52 years for the stratospheric lifetime for CFC-11 results in computed lifetimes of 34, 66, and 38 years, respectively, for halons 1211, 1301, and 2404. These values are broadly consistent with the stratospheric partial lifetimes reported by WMO 2014, given in Table 2.

3.1.2. Source Gas Injection from VSLS (SGI^{VSLS})

An important focus of CONTRAST and ATTREX was the quantification of the stratospheric supply of bromine via both SGI and PGI. Here, we used the fits of VSLS as functions of CFC-11 (Table 2) to arrive at an estimate for SGI^{VSLS} of 2.9 ± 0.6 ppt. The value of 2.9 ppt is the sum of the five values of $(X)_o$ for VSLS, and the uncertainty of 0.6 ppt is a root sum of squares combination of the fitting uncertainties for the five VSLS. This estimate combines data acquired at the top of the TTL and within the photochemically aged stratosphere in the context of a physically plausible model for the decay of the bromocarbons and mimics the approach of Wamsley et al. (1998). An alternate method to estimate SGI^{VSLS} is to tabulate the bromine content of the five VSLS compounds near 17 km in the tropics, which we quantify below.

Figure 5 compares these two approaches for estimating SGI^{VSLS}. The red diamond represents the tracer-based estimate for SGI^{VSLS} of 2.9 ± 0.6 ppt, described above. The rest of Figure 5 shows profiles of VSLS in the TWP. The square and circle symbols represent the organic bromine content of various VSLS measured during CONTRAST and ATTREX, respectively. The WAS measurements have been averaged within 1 km altitude bins, and the error bars represent the standard deviation about the mean within each bin. CONTRAST data shown in Figure 5 were acquired during twelve flights in the TWP, including portions of RF06 and RF15. The lines show calculations of profiles for these VSLS, averaged for February over the TWP, from CAM-chem-SD (Fernandez et al., 2014; Navarro et al., 2015) (Section 2.1.2).

Note that the three minor VSLS have been summed together, for both measured and modeled profiles.

Overall the observed profiles of VSLS from CONTRAST and ATTREX compare well to theoretical profiles from CAM-chem-SD in the TTL. Navarro et al. (2015) showed similarly good comparisons, based on ATTREX observations in the Western and Eastern Pacific. The CAM-chem-SD profile is slightly higher than observed for CH_2Br_2 above 15 km and for $CHBr_3$ between 11 and 14 km, leading to slightly larger modeled values for CBr_y than observed in TTL (~13 to 17 km). Below 2 km, $CHBr_3$ mixing ratios are higher in CAM-Chem-SD than the mean values observed during CONTRAST (Figure 5). A similar discrepancy exists between CAM-Chem-SD $CHBr_3$ and measurements obtained during CAST (not shown), which sampled altitudes below 8 km in the TWP during winter 2014 (Andrews et al., 2016). Previous evaluations of the Ordóñez et al. (2012) climatology, used by CAM-chem-SD for emissions of VSLS, have identified the potential to overestimate the actual emissions of $CHBr_3$ based on a comparison of model output to ground-based and Southeast Asian aircraft observations (Hossaini et al., 2013, 2016). However, CAM-Chem-SD shows excellent agreement with ATTREX measurements of $CHBr_3$ sampled at higher altitudes. Profiles of all individual VSLS and longer-lived compounds are shown in Figure S8. In this figure, WMO 2014 surface mixing ratios of CH_3Br and halons are included (Harris and Weubbles et al., 2014), demonstrating good agreement between CAM-chem-SD tropospheric and WMO 2014 surface values for halon-1301.

As noted above, some prior estimates of SGI^{VSLS} have been based on observations near 17 km. For this altitude in the TWP, the bromine content of the five VSLS observed during ATTREX is 3.4 ± 0.3 ppt (Table 3). This estimate differs slightly from the value of 3.27 ± 0.47 ppt reported by Navarro et al. (2015), because we have restricted our analysis to GWAS measurements collected within 20°S to 20°N. A comparison to the prior estimates of VSLS at 17 km in the tropics, given in Chapter 1 of WMO 2014, shows that ATTREX observations of CH_2Br_2, CH_2BrCl, and $CHBr_2Cl$ all lie within the WMO 2014 range, albeit on the upper end (Table 3). Conversely, the ATTREX 17 km mean observations of $CHBr_3$ and $CHBrCl_2$ exceed the upper range from WMO 2014. This difference could be due to our sampling of the biologically and convectively active TWP, since the WMO 2014 values are based on measurements throughout the tropics. Furthermore, the mean and standard deviation of AWAS measurements of VSLS between 10 and 12 km is 4.7 ± 0.6 ppt. This value is slightly higher than

584 but within one standard deviation of previously reported upper tropospheric values of 4.4 ± 0.4
585 ppt above Southeast Asia during the SHIVA campaign (Sala et al., 2014) and 4.2 ± 0.6 ppt
586 during an oceanic flight of CARIBIC (Wisher et al., 2014).

587 The upper limit for the uncertainty in our 2.9 ± 0.6 ppt tracer-based estimate for SGI^{VSLS}
588 (red diamond in Figure 5) encompasses the value of SGI^{VSLS} measured at 17 km during
589 ATTREX (3.4 ± 0.3 ppt, grey circle at 17 km in Figure 5). Despite the coverage of observations
590 provided by seven flights of the GH during ATTREX, it is unclear how representative the
591 measurements acquired at 17 km are of the conditions for the entire winter in the TWP. Due to
592 their short lifetimes, the transport of VSLS is expected to be highly variable in both time and
593 space. The CONTRAST campaign sampled the TTL in the TWP earlier in the winter season
594 compared to ATTREX (Jensen et al., 2017; Pan et al., 2017). For the altitude region where there
595 is overlap of these two datasets (i.e. between 14 and 15 km), the CONTRAST observations of
596 the bromine content of VSLS in the TWP are 0.3 ppt lower than measured during ATTREX
597 (Figure 5). This offset is largely due to lower $CHBr_3$ mixing ratios measured during
598 CONTRAST than ATTREX (Figure S8). Since AWAS and GWAS measurements use the same
599 calibration and GC/MS systems, this difference probably indicates that for the conditions
600 sampled during CONTRAST, there was either slightly smaller emissions or less efficient vertical
601 transport of CH_3Br than occurred for the air masses sampled later in winter at 17 km during
602 ATTREX.

603 We use the tracer-based value for SGI^{VSLS} of 2.9 ± 0.6 ppt in the analysis below. Given
604 the short lifetimes of many VSLS, we place greater emphasis on this estimate of SGI^{VSLS}, since
605 this method inherently includes air parcels with a much greater diversity of convective history.
606 For instance, the tracer-based estimates of SGI from $CHBr_3$ and CH_2Br_2 (Table 2) are both about
607 0.2 ppt lower than their 17 km means (Table 3). The tracer analysis for $CHBr_3$ is based on all
608 stratospheric ATTREX measurements in the tropics, which includes measurements around 17
609 km as well as more convectively aged air parcels at higher altitudes. Consequently, the tracer-
610 based SGI for $CHBr_3$ averages the conditions sampled by ATTREX and CONTRAST in the
611 TTL. Additionally, the tracer-based estimate for SGI of CH_2Br_2 makes use of data that span a
612 large range of latitudes and provides a more direct representation of the conditions sampled by
613 the instruments that measured BrO, which is used to calculate PGI.

3.1.3. Inorganic Bromine from SGI (Br_y^{SGI})

The bromocarbon versus CFC-11 tracer relations, defined in Section 3.1.1 are used to calculate the expected formation of Br_y following stratospheric decay of VSLS, CH_3Br and halons, which we term Br_y^{SGI}. Figure 6 illustrates our approach for estimating the expected rise of Br_y^{SGI} as a function of decay of CFC-11. This estimate of Br_y^{SGI} is an essential component for a comprehensive analysis of the bromine budget for the TWP. Here, we combine the estimate of Br_y^{SGI} with a box model analysis of measured BrO to infer PGI from VSLS (Section 3.2).

Figure 6a shows the relation between stratospheric CBr_y and CFC-11, calculated according to:

$$CBr_y = \sum (X_i)_o \left[\frac{(CFC\text{-}11)}{(CFC\text{-}11)_o}\right]^{\frac{1}{d_i}} \quad (3)$$

where the summation is performed over all bromocarbons, indicated by *i*. The two lines in Figure 6a make use of values of $(X_i)_o$ and d_i given in Table 2. Here and throughout, orange is used to represent the stratospheric supply of bromine from the decay of long-lived CH_3Br and halons and black is used to represent the supply from both VSLS and long-lived compounds. The lines show the slow decay of the bromocarbons in the LMS represented by equation (3). The squares indicate the total organic bromine content as measured by AWAS during CONTRAST, plus the CAM-chem-SD value for halon-1301. In some instances, the measurements from AWAS are incomplete (i.e., the mixing ratio for one or more of the eight AWAS compounds in Table 2 is not available). If values for either $CHBrCl_2$ or halon-1211 are missing, we used the fit parameters to estimate the abundance. This allows for more data points on Figure 6a.

Figure 6b illustrates our estimate for the appearance of inorganic bromine upon stratospheric oxidation of the organic sources. Again, our approach is the same as that of Wamsley et al. (1998). Assuming the total bromine content of the stratosphere is present either in organic or inorganic form in the gas phase (i.e., aerosol uptake and washout, within the stratosphere, are inconsequential), then the inorganic bromine (Br_y^{SGI}) provided by the oxidation of organics is represented by:

$$Br_y^{SGI} = SGI^{LL+VSLS} - CBr_y \quad (4)$$

where CBr_y is calculated according to equation (3). In equation (4), $SGI^{LL+VSLS}$ is the total bromine that entered the stratosphere in organic form: i.e., $SGI^{LL+VSLS}$ equals the sum of SGI from long-lived compounds (SGI^{LL}) and SGI^{VSLS}.

We assume the value of SGI^{VSLS} measured during CONTRAST and ATTREX campaigns is constant over time. Conversely, it is known that SGI^{LL} varies over time, and the surface mixing ratios of CH_3Br and halons have decreased slightly over the past decade due to the success of the Montreal Protocol (Figure S7). In order to represent the slow decay of CH_3Br and halons in the global troposphere, an estimate for the age of stratospheric air is needed. Age of air is the mean time an air parcel takes to travel from the base of the stratosphere to the location of measurement (Hall & Plumb, 1994). Here, the N_2O based estimate for age of air given in Engel et al. (2002) is used, tied to the CFC-11 versus N_2O relation from CAM-chem-SD and AWAS observations of CFC-11 (see Text S2 in supporting information). The mean age of air as a function of CFC-11 has been used to adjust SGI^{LL} in Figure 6b, such that the values correspond to the time series of CH_3Br and halon surface mixing ratios given in Chapter 5 of WMO 2014 (Harris and Wuebbles et al., 2014). The bromine content of SGI^{LL}, represented by the orange dotted line in Figure 6b, increases slightly from 15.0 ppt where CFC-11 is 233 ppt to 15.2 ppt where CFC-11 is 175 ppt, which reflects the slow, gradual decline of long-lived bromocarbons.

Finally, the dashed lines in Figure 6b represent the rise in inorganic bromine due to the decay of long-lived bromocarbons as a function of CFC-11 (orange) and the rise in organic bromine due to the decay of all sources that enter the stratosphere with carbon intact (black; Br_y^{SGI}). The curve for Br_y^{SGI} was found using equation (4); in simple graphical terms, Br_y^{SGI} is the difference between the black dotted and the black solid lines in Figure 6b. Similarly, the orange dashed line is the difference between the orange dotted and solid lines.

3.2. Product Gas Injection (PGI)

Here we estimate the supply of bromine to the stratosphere by inorganic species that cross the tropopause. The estimate of PGI given below is unable to distinguish between inorganic bromine produced following the decomposition of VSLS and inorganic bromine from other sources, such as sea salt aerosol. While theoretically sea salt aerosol should be most important in the lower portions of the tropical troposphere, a number of recent studies have shown this source can be important at higher altitudes, mainly within active convective regions

669 such as the TWP (Fernandez et al., 2014; Koenig et al., 2017; Long et al., 2014; Schmidt et al.,
670 2016; Wang et al., 2015; Yang et al., 2005).

671 The top panels of Figure 7 show the partitioning of gas phase Br_y compounds within our
672 constrained photochemical box model (Section 2.2) along each of the flight tracks. The bottom
673 panels display the time series of gas phase Br_y inferred from observations of BrO reported by
674 AMAX-DOAS (green) and CIMS (blue) for CONTRAST RF06 and RF15. The error bars for
675 Br_y in these panels were calculated by applying the box model BrO/Br_y partitioning to the upper
676 and lower 1σ uncertainty limits of the BrO measurements reported by the two instruments teams.
677 The value of Br_y within CAM-chem-SD, interpolated in space and time to the GV flight tracks, is
678 shown by the red lines. As the GV entered the stratosphere (black vertical dashed lines), Br_y
679 increases as expected. The value of Br_y inferred from AMAX-DOAS BrO broadly peaked
680 around 3 ppt for RF06, and Br_y inferred from both AMAX-DOAS and CIMS BrO peaks around
681 6 ppt for RF15. As noted in Section 2.1.1, observations of BrO from CIMS are not available for
682 RF06. The rise in Br_y is considerably more pronounced for RF15, reflecting deeper penetration
683 into the stratosphere. The simulation of Br_y from CAM-chem-SD exhibits overall good
684 agreement with Br_y inferred from BrO and related observations during the middle portion of
685 RF15 where the aircraft sampled the deeper in the stratosphere, and mixing ratios of O_3 are
686 above 200 ppb.

687 The largest difference between Br_y inferred from AMAX-DOAS and CIMS occurs near
688 the edges of the stratosphere (Figure 7d). The CAM-chem-SD value for Br_y nearly splits the
689 difference between the estimates based on AMAX-DOAS and CIMS BrO, similar to the
690 comparison of BrO shown in Figure 3h. We base our best estimate of PGI on a statistical
691 analysis of both measurements, since we have no basis for assessing which observationally-
692 based estimate of Br_y is more likely to be correct. Finally, the fact that the CAM-chem-SD
693 estimate for BrO shown in Figure 3h looks nearly identical compared to observations as the
694 CAM-chem-SD estimate for Br_y shown in Figure 7d demonstrates that the representation of the
695 BrO/Br_y ratio is comparable between our photochemical box model and the global model (Figure
696 S9). Koenig et al. (2017) highlight large variations in the Br_y partitioning obtained with both box
697 and global models in the upper troposphere, outside of the regions used here, particularly where
698 aerosol SAD is below 1×10^{-8} cm^2 cm^{-3}. This suggests that further research regarding transport,
699 recycling, and/or washout of inorganic bromine is still required.

Our estimate of PGI is based on inferred Br_y only within the stratosphere. As the GV aircraft travels deeper into the stratosphere, the BrO/Br_y ratio increases during both RF06 and RF15, due to the declines in atomic Br and HBr, driven by ambient O_3 and heterogeneous processing. This behavior is consistent with the explanation for bromine partitioning described by Fernandez et al. (2014) and Koenig et al. (2017). Within the stratosphere, the contribution of $BrONO_2$ to the Br_y budget increases as the mixing ratio of O_3 exceeds 200 ppb (middle portion of Figure 7b) and NO_2 exceeds 50 ppt (Figure S2a). As discussed below, Br_y inferred for this flight segment is sensitive to the accuracy of the kinetic information used to define the rates of formation and loss of $BrONO_2$, which currently has considerable uncertainty (Kreycy et al., 2013; Sioris et al., 2006). Most importantly, our estimate of PGI is weighted towards flight segments for which BrO constitutes about half of Br_y.

The relationship between the inferred Br_y and AWAS CFC-11 was used to estimate PGI (Figure 8). Five minute averages of stratospheric Br_y, inferred from BrO observations, were calculated at the time of each AWAS CFC-11 measurement. PGI was calculated from the mean difference between Br_y^{SGI} (black line in Figure 8) and inferred Br_y. The PGI estimate using both AMAX-DOAS and CIMS measurements is 2.1 ± 1.3 ppt, where the reported uncertainty is the standard deviation of the mean (Figure 8a). PGI estimated using only AMAX-DOAS measurements is 2.2 ± 1.3 ppt (Figure 8b) and using only CIMS measurements is 1.7 ± 1.3 ppt (Figure 8c).

The overall PGI estimate was determined to be 2**.1** ± 2.**1** ppt, where the uncertainty is the root sum of squares combination of the 1σ uncertainties in standard deviation of the PGI estimate using both AMAX-DOAS and CIMS measurements (1.3 ppt) and the propagation of the BrO measurement uncertainties to inferred Br_y, which includes three factors: the uncertainty of BrO, the impact of JPL 2015 kinetic uncertainties on the BrO/Br_y ratio, and uncertainties in observations other than BrO used to constrain the box model (Table S2). Of these factors, the largest contribution (~1.3 ppt) to the overall uncertainty in PGI (2.1 ppt) is the uncertainty in measured BrO (error bars in Figure 3g and 3h). The impact of chemical kinetics on our estimate of PGI is driven by the uncertainty in the rate constant of $BrO + NO_2 + M$, given in JPL 2015.

Ambient NO_2 makes the third largest contribution to the uncertainty in PGI. In our base scenario, modeled NO_y is constrained by AMAX-DOAS measurements of NO_2 (Section 2.2). If modeled NO_y is instead constrained to chemiluminescence measurements of NO, the PGI

731 estimate decreases by 0.6 ppt due to decreasing mixing ratios of NO_2 within the box model.
732 Further details are provided in Figure S2a of supporting information and figure S1 of Koenig et
733 al. (2017). Consequently, the lower limit of our PGI estimate includes the uncertainties
734 introduced by constraining modeled NO_y to chemiluminescence NO. Additional information
735 regarding our estimate of the uncertainty in PGI is given in supporting information (Text S3,
736 Figure S10).
737 Additionally, the analysis presented in this section and in Section 3.1 was repeated using
738 a dynamical definition of the tropopause (2 PVU, green lines in Figure 1) instead of the thermal
739 tropopause. With the dynamical tropopause, the resulting SGI^{VSLS} increases to 3.0 ± 0.7 ppt and
740 the PGI decreases to 1.7 ± 2.0 ppt, which is within the overall uncertainties calculated using the
741 thermal tropopause.
742 Values of Br_y inferred from the AMAX-DOAS measurements of BrO levels off, with
743 respect to CFC-11, for mixing ratios of CFC-11 below about 210 ppt **(**green squares, Figure 8).
744 This behavior is contrary to the theoretical expectation that Br_y should rise as CFC-11 declines.
745 The lowest mixing ratios of CFC-11 are accompanied by sharp positive spikes in O_3 (Figure 3d).
746 As discussed in Section 2.1.1, since the AMAX-DOAS instrument collects differential slant
747 column density measurements of BrO horizontally in front of the plane and in a narrow band
748 above and below the aircraft, it is possible that the sharp gradients in atmospheric composition,
749 as observed by the in situ AWAS and chemiluminescence instruments, are not captured by the
750 remote sensing AMAX-DOAS instrument. Conversely, since high levels of O_3 can interfere with
751 the CIMS measurements, sharp atmospheric gradients can also affect the in situ observations.
752 Furthermore, for locations where peak O_3 and NO_2 are observed, the impact of kinetic
753 uncertainties on $BrONO_2$ kinetics increases. Consequently, we use the combination of the
754 AMAX-DOAS and CIMS observations of BrO to calculate Br_y^{VSLS} and PGI.
755 The 2.1 ± 2.1 ppt PGI estimate presented here is in good agreement with previous
756 ATTREX and CONTRAST studies. In the Navarro et al. (2015) analysis of ATTREX GWAS
757 measurements, CAM-chem-SD was used to estimate PGI. In their study, output from the CAM-
758 chem-SD model was used to estimate a value for PGI of 1.97 ± 0.21 ppt. Our observational
759 based estimate is nearly identical, albeit with larger uncertainty. The two previous studies that
760 analyzed CONTRAST measurements of BrO restricted their estimates of PGI to analysis of data
761 collected in the upper troposphere and the bottom of the stratosphere (i.e. where O_3 < 200 ppb

and the observed ratio of H_2O/O_3 < 0.1 ppm/ppb). The PGI estimate presented in Koenig et al. (2017) is 2.6 ± 0.6 ppt based on remotely sensed AMAX-DOAS measurements and is slightly higher than our estimate of 2.2 ± 1.3 ppt (Figure 8b) based on analysis of all AMAX-DOAS data collected for altitudes above the thermal tropopause. Chen et al. (2016) estimated a PGI of approximately 2 ppt based on Br_y inferred from in-situ CIMS observations of BrO acquired for air parcels where O_3 is between 100 and 200 ppb, which is in agreement with the 1.7 ± 1.3 ppt estimate (Figure 8c) presented here based on our analysis all of CIMS BrO acquired in the stratosphere. Our study is the first to present a single estimate for PGI by combining measurements of BrO obtained by both the AMAX-DOAS and CIMS instruments during CONTRAST.

3.3. Stratospheric Bromine from VSLS (Br_y^{VSLS})

The total contribution of VSLS to stratospheric bromine is found by combining our SGI^{VSLS} (2.9 ± 0.6 ppt) and PGI (2.1 ± 2.1 ppt) estimates, yielding 5.0 ± 2.1 ppt of Br_y^{VSLS}. The uncertainties in the SGI^{VSLS} and PGI estimates are not additive, since a decrease in SGI^{VSLS} would cause a corresponding increase in PGI based on our method. Overall uncertainty in Br_y^{VSLS} is dominated by the uncertainty in our estimate of PGI. The smaller range of values for PGI and Br_y^{VSLS} are true if: (a) the lower limits of the uncertainties in measurements of BrO are more accurate; (b) the kinetics governing the formation of $BrONO_2$ are faster than the JPL 2015 recommendation; (c) and/or nitrogen oxide loading is better represented by chemiluminescence NO than by AMAX-DOAS NO_2. Conversely, the larger values of PGI and Br_y^{VSLS} are true if: (a) the upper limits of the uncertainties in measurements of BrO are more accurate, (b) the kinetics governing the formation of $BrONO_2$ are slower than the JPL 2015 recommendation, (c) and/or nitrogen oxide loading is better represented by AMAX-DOAS NO_2 than by chemiluminescence NO.

Our 5.0 ppt best estimate of Br_y^{VSLS} is in perfect agreement with the value given by WMO 2014; however, our ± 2.1 ppt uncertainty is smaller than the WMO 2014 uncertainty of ± 3 ppt. In addition to observed SGI^{VSLS} and modeled PGI, estimates of Br_y^{VSLS} in WMO 2014 have been based on analysis of BrO profiles in the middle to upper stratosphere obtained by either ground-based (e.g., Schofield, 2004; Theys et al., 2007), balloon-borne (e.g., Dorf et al., 2008; Stachnik et al., 2013), or satellite instruments (e.g., Dorf et al., 2006; Sioris et al., 2006; Kovalenko et al., 2007; McLinden et al., 2010; Parrella et al., 2013). The mean value of the best

estimate for Br_y^{VSLS} from these studies is 6 ppt, with a range of 3 to 8 ppt (Carpenter and Reimann et al., 2014). If a modification to the kinetics that govern the $BrONO_2$ to Br_y ratio put forth based on atmospheric observations reported by Kreycy et al. (2013) is adopted, these values fall to a best estimate of 5 ppt, with a range of 2 to 8 ppt. This proposed kinetic revision would decrease our Br_y^{VSLS} estimate by 0.5 ppt and is considered in our overall uncertainty (Text S3).

Also, our estimate is in excellent agreement with the 5.2 ± 2.5 ppt value for Br_y^{VSLS} given by Dorf et al. (2008) based on analysis of balloon-borne observations acquired at Teresina, Brazil (5.1° S, 42.9° W) during June 2005. Dorf et al. (2008) estimated that a larger portion of the stratospheric transport of VSLS occurred as inorganic bromine (PGI = 4.0 ± 2.5 ppt) than found in our study. They also ascribed the same uncertainty to both Br_y^{VSLS} and PGI (i.e. ± 2.5 ppt), since organic bromine species are able to be measured with much better accuracy and precision than can be achieved for BrO. The need to infer total inorganic bromine from measured BrO adds an additional, important source of uncertainty (e.g. Kreycy et al., 2013) to estimates of both PGI and Br_y^{VSLS}.

4. **Comparison to CCMI Models**

4.1. Model descriptions

Output from 14 global models involved in CCMI (Eyring et al., 2013; Morgenstern et al., 2017b) were analyzed to assess the representation of the stratospheric supply of bromine from VSLS (Table 4). Thirteen of these models are chemistry-climate models (CCMs) that rely on internal, model generated transport fields, whereas TOMCAT is a chemical transport model (CTM) that uses fields from observed meteorology. Additionally, three simulations of the EMAC CCM were considered. The EMAC-L47MA and EMAC-L90MA simulations use internally generated meteorological fields with 47 and 90 pressure levels, respectively. The EMAC-L90MA-SD simulation, which uses observed meteorology and 90 pressure levels, was examined to assess the effect of observed versus internally generated meteorology on the results of this study. The inclusion of EMAC in the multi-model mean analysis is based on the average of the three simulations, before combining with other models, so that EMAC does not have undue influence on the resulting multi-model mean. Finally, meteorological fields specific for winter 2014 were used to drive the TOMCAT and EMAC-L90MA-SD simulations shown below.

For the CCMs considered in this study we have used monthly, zonal mean output of organic and inorganic bromine compounds as well as CFC-11 and tropopause pressure for January through March 2014 from the Ref-C2 scenario. These variables have been archived by the CCMI project and are maintained either by the NCAR Earth System Grid (CESM1-CAM4Chem and WACCM) or the British Atmospheric Data Centre (all other CCMs). The EMAC-L90MA-SD and TOMCAT CTM variables are zonally resolved, monthly mean output and were shared privately. The Ref-C2 simulations utilize the surface mixing ratios of ozone depleting substances given by the A1 scenario from the 2010 WMO Ozone Assessment (Montzka and Reimann et al., 2010). Morgenstern et al. (2017) provides a high-level description of the global models involved in CCMI.

The CCMI models are grouped according to how they represent Br_y^{VSLS}. As listed in Table 4, nine of the models provide an explicit simulation of at least the two major VSLS ($CHBr_3$ and CH_2Br_2). The majority of the CCMs that explicitly represent VSLS impose a 1.2 ppt surface mixing ratio for both CH_2Br_2 and $CHBr_3$, as suggested by Eyring et al. (2013). The surface loading of VSLS from Eyring et al. (2013) was designed to result in 4.5 to 5.0 ppt of Br_y^{VSLS}, since washout was expected to remove a fraction of the inorganic gases produced by oxidation of VSLS in the troposphere. The EMAC model and TOMCAT CTM are exceptions among the explicit CCMI models for their treatment of Br_y^{VSLS}. In addition to CH_2Br_2 and $CHBr_3$, the EMAC simulations include bromine sources from sea salt aerosols and three minor VSLS (CH_2BrCl, $CHBr_2Cl$, and $CHBrCl_2$). Also, biogenic emissions of VSLS in EMAC emissions are parameterized according to Warwick et al. (2006). Within TOMCAT the surface mixing ratios of $CHBr_3$ and CH_2Br_2 are each 1 ppt. Finally, the implementation of sources of VSLS in the CESM1 CAM4-Chem version included in CCMI follows Eyring et al. (2013), while the CAM-chem-SD version used in Section 2.1.2 to analyze CONTRAST and ATTREX observations relied on the Ordóñez et al. (2012) emission scenario.

The last five CCMs listed in Table 4 utilize a simpler treatment for VSLS. Within these models, the surface mixing ratio of CH_3Br was increased by 5 ppt to represent the bromine loading from VSLS. This surrogate method was described by Eyring et al. (2013) as an option for modeling groups that did not have the resources to add explicit treatment of VSLS. The surface mixing ratio of CH_3Br was increased by 5 ppt since tropospheric loss of this compound, which is longer-lived than VSLS, is expected to be small.

We have included all CCMI models that have archived model output for CBr_y, Br_y, and CFC-11 for winter 2014. Except for the TOMCAT CTM and EMAC-SD simulation, the model results are not based on observed transport fields and hence are not expected to match the actual meteorological conditions. However, due to changing anthropogenic emissions and regulation by the Montreal Protocol, the surface mixing ratios of CH_3Br and halons change over time. To assess the model representation of the bromine loading observed during the CONTRAST and ATTREX campaigns, outputs from all of the CCMI models were analyzed only for the time period January to March 2014.

4.2. Multi-Model Means

The goal of CCMI is to evaluate and improve the behavior of global models that have been designed to assess the interactions between climate change and atmospheric chemistry (Eyring et al., 2013; Morgenstern et al., 2017b). Many scientific studies that utilize CCMI models have focused on stratospheric ozone (e.g. Fernandez et al., 2017; Oman et al., 2016; Sinnhuber & Meul, 2015). Since realistic representation of bromine is necessary to properly simulate stratospheric ozone, we compare the bromine loading in 14 CCMI models (Table 4) to the empirical estimate based on CONTRAST and ATTREX observations. Each CCMI model is classified as either having "explicit" or "surrogate" treatment of VSLS, according to how the model simulates VSLS.

Multi-model means of bromine as a function of CFC-11 from explicit and surrogate models are shown in Figure 9. The modeled CBr_y, Br_y, and total bromine (CBr_y + Br_y) have been averaged within 10 ppt bins of modeled CFC-11. The multi-model mean bromine loading of the nine CCMI models listed in Table 4 that explicitly model VSLS are shown in Figure 9a, and the multi-model means of the five surrogate models are shown in Figure 9b. To properly compare observed and modeled bromine using CFC-11, model output for CFC-11 is scaled by the ratio of observed to modeled CFC-11 at the tropical tropopause (Table S4). Since the variation of CBr_y compounds with CFC-11 is expected to be different in the tropics than in the extratropics (Volk et al., 1996), and the majority of the observations used in our study were obtained in the northern extratropics, model output was filtered to include output poleward of 30°N and between the model tropopause pressure and 1 hPa. Similar figures for all individual explicit and surrogate models are discussed in Section 4.3.

The three observed bromine relations (total, organic decay, and inorganic rise) are shown in grey as functions of CFC-11 in Figure 9. The observed CBr_y relation is based on the solid black line shown in Figure 6b, extended to lower mixing ratios of CFC-11 using equation (3) as well as the values of d and $(X)_o$ given in Table 2. The observed Br_y relation represents inorganic bromine that forms upon stratospheric decay of all CBr_y compounds (equation 4, lower limit of grey shading) plus the amount of inorganic product gas that is transported across the tropopause (PGI = 2.1 ± 2.1 ppt). For comparison, an additional orange line is shown in each panel to indicate the expected Br_y relation due to supply from only halons and CH_3Br (equation 4, orange dashed lines in Figure 6b). Finally, total bromine is the sum of observed CBr_y and Br_y. The grey shaded regions in Figure 9 show the upper and lower bounds of the three observed bromine relations, where the range in CBr_y is defined according to the uncertainty reported in Table 2 (vertical error bars in Figure 6b). The limits of the grey shaded regions for Br_y and for total bromine are both defined according to the 0.0 to 4.2 ppt range in estimated PGI. Finally, since the lowest mixing ratio for CFC-11 observed during CONTRAST was 188 ppt, bromine relations at lower mixing ratios of CFC-11 are extrapolated and shown using dashed lines. These extrapolations are based on equations (3) and (4), following an approach that is commonly used to relate aircraft observations to global model output (e.g. Wamsley et al., 1998).

Figure 9a shows results from the multi-model mean of CCMI models with explicit representation of VSLS. The values of CBr_y and Br_y in these models follow the observed curvature of the respective observed bromine versus CFC-11 relations quite well. However, the values of Br_y tend to lie either close to the central values of our empirical estimate or along the upper limit of the range for all levels of CFC-11. The similarity between the modeled and observed relations implies that mean SGI^{VSLS} and PGI in explicit models are similar to that determined using CONTRAST and ATTREX data.

Table 5 compares the multi-model mean and standard deviation of SGI and PGI from the CCMI models, separated based on explicit and surrogate of VSLS, to values of SGI and PGI inferred from the field observations. For this table, SGI^{LL} and SGI^{VSLS} were calculated from the sum of long-lived substances and VSLS at the tropopause pressures, reported by the global models, within the tropics (20°S to 20°N). Likewise, PGI and total bromine were calculated from the mixing ratios of modeled Br_y and the sum of modeled organic and inorganic bromine,

913 respectively, at the tropical tropopause. Multi-model mean values are highlighted in bold and
914 results for individual models are discussed in Section 4.3.

915 The mean value of SGI^{VSLS} for the explicit models is 2.8 ± 1.1 ppt, which is close to the
916 observed value of 2.9 ± 0.6 ppt (Table 5). The mean value of PGI for these models is 3.6 ± 0.9
917 ppt, which is larger than the observed value of 2.1 ± 2.1 ppt but within the range of uncertainty.
918 As shown in the next section, all nine models with explicit treatment of VSLS estimate higher
919 PGI than observed. This reflects the tendency of the modeled Br_y to be along upper range of
920 observations in Figure 9a. The CCMI model representation of PGI depends on the rate of
921 decomposition of organic bromocarbons in the tropical troposphere (e.g. Rex et al., 2014), the
922 efficiency of heterogeneous reactions controlling the uptake and labile release of inorganic
923 bromine species (e.g. Sinnhuber and Folkins, 2006), as well as the efficacy of the sea-salt
924 dehalogenation source (e.g. Schmidt et al., 2016; Wang et al., 2015). Further research is required
925 to understand the role of these factors in driving the differences of computed PGI shown in Table
926 5, as well as the tendency for all of the models to exceed our central empirical estimate of 2.1
927 ppt.

928 The bromine relations in CCMI models with surrogate VSLS are shown in Figure 9b.
929 Since CH_3Br has a longer photochemical lifetime than VSLS in the lower stratosphere, the decay
930 of CBr_y with decreasing mixing ratios of CFC-11 is slower in these models compared to both
931 observation (Figure 9b) and CBr_y from models that use an explicit treatment (Figure 9a).
932 Consequently, Br_y in the surrogate CCMI models most commonly lies along the lower limit of
933 the empirical range of the Br_y versus CFC-11 relation, particularly in the lower stratosphere (i.e.,
934 for the highest mixing ratios of CFC-11). As a result, these models could underestimate the role
935 of bromine in photochemical loss of ozone in this region of the atmosphere. For older air parcels
936 (i.e. low mixing ratios of CFC-11), Br_y in the surrogate models resembles the observed Br_y
937 versus CFC-11 relation fairly well, due to the release of bromine contained in CH_3Br.

938 The entries for the surrogate models in Table 5 list numerical values only for SGI^{LL}, PGI,
939 and total bromine. For these models the entry for SGI^{LL} represents source gas injection by all
940 organic compounds, since VSLS are not explicitly simulated. The models with surrogate
941 treatment of VSLS exhibit a PGI of 1.0 ± 0.3 ppt, which is lower than both the observed value of
942 2.1 ± 2.1 ppt as well as that found by the explicit models, 3.7 ± 0.9 ppt. This tendency is due to

the relatively long tropospheric lifetime of CH_3Br compared to $CHBr_3$, and demonstrates a potential shortcoming in the surrogate treatment of VSLS.

The mean total bromine loading of 20.3 ± 1.5 ppt in the explicit models as well as the 20.0 ± 1.0 ppt in the surrogate models are both close to the 20.0 ± 2.1 ppt observed value (Table 5). Furthermore, for more photochemically aged air (i.e. CFC-11 less than ~120 ppt), the representation of Br_y in surrogate models is within the observed range (Figure 9b). Consequently, the representation of stratospheric bromine for studies of polar ozone should be reliable for both explicit and surrogate treatments of VSLS. As discussed above, the orange lines in Figure 9 are the observed Br_y relation supplied by halons and CH_3Br (equation 4). All CCMI models that use explicit or surrogate representations of VSLS lie much closer to the empirical estimate of Br_y from CH_3Br, halons, and VSLS (grey) than to the estimate using only CH_3Br and halons (orange). As a result, both CCMI methods for including VSLS are able to more closely simulate observed stratospheric bromine than would be found if VSLS had been completely neglected.

Our estimates for stratospheric bromine injection in Table 5 are calculated using the tropopause values throughout the tropics from the CCMI models. Since the archived model output represents the entire tropical tropopause, use of this archived output is the most convenient and meaningful way to determine SGI and PGI. Because the output from the majority of the CCMs are only available as zonal means, we are not able to separate the contribution of the TWP. The precise values for SGI and PGI within the CCMs can depend on details of the meteorological fields. However, a comparison between two EMAC simulations that used an internally generated transport field and an EMAC run that relied on observed meteorology revealed no discernable difference in the resulting bromine relations in the middle and upper stratosphere and a small difference, well within the observational uncertainty, for the LMS (Text S4 and Figure S11). Furthermore, values of SGI and PGI from the CCMI models calculated using the tracer-tracer relation approach are similar to those given in Table 5 (Text S5 and Table S5).

Previous studies have evaluated the ability of different emission inventories of VSLS to represent stratospheric bromine injection. Our estimates for SGI^{VSLS} of 2.9 ± 0.6 ppt (observed) and 2.8 ± 1.1 ppt (explicit CCMI models) (Table 5) are slightly higher than the SGI^{VSLS} value of 2.0 ppt (range 1.2 to 2.5 ppt) reported by Hossaini et al. (2016). Additionally, our values for

974 Br_y^{VSLS} of 5.0 ± 2.1 ppt (observed) and 6.4 ±1.4 ppt (explicit models) are both well within the 4
975 to 8 ppt range reported by Hossaini et al. (2013). While the global models considered in the
976 Hossaini et al. (2016) and Hossaini et al. (2013) studies use observation-based emission
977 inventories for VSLS (Liang et al., 2014; Ordóñez et al., 2012; Ziska et al., 2013), the CCMI
978 models (with the exception of EMAC) use a more simplified approach of prescribed surface
979 mixing ratios of VSLS. It is therefore reassuring that this simplified approach is able to
980 adequately represent stratospheric injection of VSLS. Explicit representation of oceanic
981 emissions of VSLS provides an avenue for assessing the impact of climate change and oceanic
982 biology on atmospheric bromine that is inaccessible upon use of prescribed mixing ratios (Falk et
983 al., 2017; Lennartz et al., 2015). Our analysis of the aircraft observations in the TWP, such as the
984 grey curves in Figure 9, provide a benchmark for evaluation of the modeled representation of
985 stratospheric bromine within global models.

986 4.3. Individual Models

987 Figure 10 shows bromine relations from all CCMI models with explicit treatment of
988 VSLS. Each panel was prepared in the same manner as Figure 9, and the panel for EMAC uses
989 the mean of the three simulations shown in Figure S11. Three of the CCMI models with explicit
990 representations of VSLS (ACCESS, CCSRNIES, and NIWA-UKCA) have CBr_y mixing ratios
991 that lie a few ppt below the observed relation. However, for all three of these models, total
992 bromine lies within the observed range of uncertainty. Table 5 also includes SGI^{VSLS} values for
993 each individual CCMI model. Of the CCMI models with explicit VSLS, values of SGI^{VSLS} in
994 WACCM, CMAM, SOCOL3, and TOMCAT are within the observed 2.9 ± 0.6 ppt range.
995 Additionally, the values of SGI^{VSLS} in all three EMAC simulations are about 2 ppt above the
996 observed central value. The tropical tropopause value of SGI^{VSLS} in the remaining four models
997 with explicit treatment (ACCESS, CCSRNIES, CAM4Chem, NIWA-UKCA) are 0.7 ppt to 1 ppt
998 below the observed central value. All explicit models, except EMAC and TOMCAT, follow the
999 same boundary conditions for VSLS from the Eyring et al. (2013) emission scheme.
1000 Consequently, the differences in SGI^{VSLS} between these models are due to model variations in
1001 the convective lofting, chemical removal (i.e. reaction with OH and loss by photolysis), and
1002 efficient washout of these compounds in the tropical troposphere.

1003 The EMAC simulations rely on geographical oceanic emission fields for $CHBr_3$, CH_2Br_2,
1004 and minor VSLS from Warwick et al. (2006). As a result, offsets between SGI^{VSLS} from the

EMAC simulations and the other CCMI models are at least partially due to differences in how the tropospheric behaviors of the source gases are simulated. Mixing ratios of $CHBr_3$ modeled using the Warwick et al. (2006) emissions have been shown to exceed observed values in Southeast Asia, which led to a suggested downward revision in the local rate of emission (Pyle et al., 2011). The observations considered by Pyle et al. (2011) were collected near the location sampled during CONTRAST and ATTREX. Therefore, the tendency for CBr_y from EMAC to lie above our observed value (Figure 10) will likely be resolved upon application of the downward revision in the emission of $CHBr_3$.

As discussed in Section 4.2, the multi-model mean Br_y (Figure 9a) and PGI (Table 5) in explicit models are within upper portion of the observed range. Similarly, in Figure 10 the values of Br_y from the explicit models tend to lie either close to the central values of our empirical estimate (CCSRNIES, CAM4Chem, WACCM, CMAM, and TOMCAT) or along the upper limit of the range (ACCESS, EMAC, NIWA-UKCA, and SOCOL3). CAM4Chem and WACCM both rely on the Community Earth System Model (CESM) framework, which we have also used to define the Halon-1301 versus CFC-11 relation, because Halon-1301 was not measured during CONTRAST and ATTREX. Since Halon-1301 supplies 3.24 ppt to the bromine budget, this could contribute to the similarity between the results from these models and our estimated Br_y versus CFC-11 relation. Additionally, CH_3Br in ACCESS, CMAM, and NIWA-UKCA was scaled to represent halon loading (Stone et al., 2016). Since CH_3Br has a shorter photochemical lifetime than halons (Table 2), the use of CH_3Br to represent halons likely results in faster release of Br_y in these models, contributing to higher Br_y loading in the lower stratosphere.

The representations of PGI in CCSRNIES, SOCOL3, and all EMAC simulations are 0.4 to 1.3 ppt larger than the observed upper limit of 4 ppt (Table 5). As a result, the Br_y loadings in these models fall along the upper limit of the observed Br_y versus CFC-11 relation at the base of the stratosphere (i.e. where CFC-11 = 230 ppt in Figure 10). However, because SGI^{LL} and SGI^{VSLS} are both low in CCSRNIES compared to other models as well as observations, inorganic bromine loading in CCSRNIES agrees well with observations. The higher value of PGI in EMAC is due to the use of emission fields from Warwick et al. (2006), as explained above for the discussion of SGI^{VSLS}. The SOCOL3 simulation has the largest value of PGI (5.3 ± 0.5 ppt), which lies above the observed upper limit of 4 ppt. For SOCOL3 and EMAC, the Br_y versus CFC-11 relations lie at or just above the upper range of our uncertainty.

The bromine relations in individual surrogate models is shown in Figure 11. Comparisons between these models and the observed bromine relations are consistent with the discussion provided in Section 4.2. Furthermore, the total bromine loading in four of the surrogate models (CNRM-CM5.3, GEOSCCM, MRI, and UMSLIMCAT), given in the last column of Table 5, is close to the 20.0 ± 2.1 ppt estimate based on CONTRAST and ATTREX observations. For these four models, the representation of stratospheric bromine for studies of polar ozone should be reliable. Based on the mean mixing ratio at the tropical tropopause, the total bromine loading in ULAQ is 18.4 ± 0.2 ppt, which is at the lower limit of the range of uncertainty. However, within the stratosphere, total bromine loading in ULAQ exhibits scatter around 20 ppt (orange squares in Figure 11), which is much closer to the observed best estimate. Furthermore, PGI and total bromine loading in ULAQ calculated using the tracer-tracer relation method are about 2 ppt larger than found using model output at the tropical tropopause (Table S5). This discrepancy between the two approaches for estimating stratospheric injection of bromine is unique to ULAQ, and is presently not understood.

5. Conclusions

The combined organic and inorganic bromine measurements collected during the CONTRAST and ATTREX aircraft campaigns in the Tropical Western Pacific (TWP) during winter 2014 provide a unique opportunity to study the contribution of VSLS to stratospheric bromine. The TWP is a region of strong convection and is the dominant pathway for short-lived compounds to reach the stratosphere, particularly during boreal winter. The payloads onboard the CONTRAST and ATTREX aircrafts included instruments that measured BrO, a suite of long-lived bromocarbons, VSLS, many other chemical constituents critical to our analysis (i.e. O_3, NO, NO_2, CFC-11, H_2O, CO, CH_4), as well as spectral actinic flux and aerosol surface area density. Data from the CONTRAST and ATTREX campaigns provide the first opportunity to quantify the gas phase bromine budget, across the tropical tropopause layer and extending into the lowermost stratosphere of the critically important TWP, in a comprehensive manner that includes direct observations of organic and inorganic bromine species.

Empirical relations between bromocarbons and CFC-11, a tracer of photochemical aging across the tropopause, were developed using whole air sampler measurements. These bromocarbon-tracer relations were used to quantify the stratospheric injection of long-lived substances and VSLS in organic form (source gas injection, SGI). Based on this analysis, the

contribution to stratospheric bromine from VSLS (SGI^{VSLS}) was determined to be 2.9 ± 0.6 ppt. This estimate is slightly lower than the 3.4 ± 0.3 ppt bromine content of organic VSLS observed at the average cold-point tropopause height (17 km) in the TWP during ATTREX. We give 2.9 ± 0.6 ppt as our best estimate for SGI^{VSLS} because this value, found using the tracer-based approach, is based on analysis of data collected in the stratosphere that incorporates air-masses with a wider range of convective histories. Both of our estimates for SGI^{VSLS} exceed the best estimate of 1.4 ppt given in WMO 2014 (Carpenter and Reimann et al., 2014), which was based on prior observations near the tropical tropopause. Our estimates do, however, lie within the upper range of the 0.7 to 3.4 ppt uncertainty for SGI^{VSLS} given in WMO 2014.

Two flights during CONTRAST sampled the extratropical stratosphere by crossing the subtropical jet off the coast of Japan. Observations of BrO obtained during these flights by two instruments, AMAX-DOAS (Koenig et al., 2017) and CIMS (Chen et al., 2016), were combined with a photochemical box model to yield estimates of gas phase Br_y. This empirical estimate of Br_y was combined with observations of long-lived bromocarbons and VSLS to estimate the stratospheric injection of bromine that crosses the tropopause in inorganic form (product gas injection, PGI). Our best estimate of PGI is 2.1± 2.1 ppt. The use of empirical bromocarbon-tracer relations builds on previous CONTRAST and ATTREX studies by providing a method for estimating PGI that considers the stratospheric decay of source gases and is applied to a large ensemble of stratospheric air masses. In the TWP, PGI represents both the decomposition products of brominated VSLS as well as transport of labile inorganic species produced by brominated sea salt throughout the troposphere. Our value is within the 1.1 to 4.3 ppt range for PGI given by WMO 2014, which was largely based on model estimates of the whole tropical region. The largest contributor to the overall uncertainty in our estimate of PGI is the measurement uncertainties of BrO. Uncertainties in the measured mixing ratios of nitrogen oxides as well as the JPL 2015 evaluation of the BrO + NO_2 + M rate constant lead to modest, additional uncertainties in PGI. Our estimate of PGI rises to 2.2 ppt upon use of BrO observations only from AMAX-DOAS, and falls to 1.7 ppt considering data only from CIMS. Observations of BrO from both instruments exhibit considerable deviation about the respective means, which also contributes to the overall uncertainty in PGI.

Our best estimate for the total contribution of VSLS to stratospheric bromine (Br_y^{VSLS}) is 5.0 ± 2.1 ppt. This estimate is in excellent agreement with the 5 ± 3 ppt assessed value given in

WMO 2014. The uncertainty in Br_y^{VSLS} is also dominated by measured BrO. The value for Br_y^{VSLS} given in WMO 2014 is mainly based on model estimates of BrO near the tropical tropopause as well as stratospheric slant column measurements of BrO. There are large uncertainties in calculating BrO near the tropical tropopause due to: aerosol uptake and washout (e.g. Sinnhuber and Folkins, 2006); spatial distribution of biogenic emissions of VSLS (e.g. Hossaini et al., 2013); the strength of convection (e.g. Fernandez et al., 2014); the efficiency of removal of VSLS by OH (e.g. Rex et al., 2014); and the production of labile bromine from sea salt aerosol (e.g. Schmidt et al., 2016). Given these uncertainties, an empirically based estimate for PGI based on measured BrO in the Western Pacific constitutes a significant step forward in our understanding of the effect of oceanic biology on stratospheric composition.

Our best estimate of Br_y^{VSLS} of 5.0 ppt is perfectly aligned with the WMO 2014 value. However, we apportion a larger fraction of the stratospheric transport of VSLS to source gases (2.9 ppt versus the WMO 2014 value of 1.4 ppt). The consistency of our two estimates of SGI^{VSLS} (2.9 ± 0.6 ppt using tracer-based approach; 3.4 ± 0.3 ppt based on sampling at the cold-point tropopause in the TWP) further supports the notion that cross tropopause transport of brominated VSLS is higher than given in the WMO 2014 assessment.

We have also provided a comprehensive comparison to the representation of brominated VSLS within 14 global models that participated in CCMI (Morgenstern et al., 2017b). The CCMI models that have explicit treatment of VSLS simulate SGI^{VSLS} in a manner that is in very good agreement with observations. These models also represent PGI that is either close to our best empirical estimate or near the upper range of the observed uncertainty. Conversely, CCMI models that have surrogate treatment of VSLS (i.e. longer-lived CH_3Br is used as a proxy for VSLS) simulate stratospheric injection of Br_y that is close to the lower range of our observationally-constrained estimate. The difference between explicit and surrogate treatment of VSLS is driven by slower decay of CH_3Br relative to VSLS.

The representation of total stratospheric bromine within CCMI models is significantly improved upon consideration of either treatment of VSLS. The multi-model mean of total bromine within explicit and surrogate models is 20.3 ± 1.5 ppt and 20.0 ± 1.0 ppt, respectively, in excellent agreement with the 20.0 ± 2.1 ppt expected based on our observations. Methyl bromide and halons, the traditional long-lived sources, provided about 15 ppt of total bromine to the stratosphere in winter 2014. Therefore, either representation of VSLS provides a

demonstrable, significant improvement over previous versions of these models that neglected the effect of VSLS on stratospheric bromine. The current formulation of bromine within the CCMI models should therefore provide more reliable simulations of the recovery of the Antarctic ozone hole (Fernandez et al., 2017; Oman et al., 2016), the effect of volcanic activity on midlatitude ozone (Feng et al., 2007; Klobas et al., 2017; Salawitch et al., 2005), the impact of geoengineering of climate on ozone (Tilmes et al., 2008, 2012), and tropospheric residual BrO inferred from satellite observations (Choi et al., 2012; Salawitch et al., 2010; Theys et al., 2011) compared to coupled chemistry-climate simulations that supply of stratospheric bromine from only CH_3Br and halons.

Acknowledgments, Samples, and Data

We sincerely appreciate the helpful comments from three, anonymous reviewers that have led to a substantial improvement in the paper. PAW, RJS, TPC, JMN, and DCA received support from the National Science Foundation (NSF), the National Aeronautics and Space Administration (NASA) Atmospheric Composition Modeling and Analysis Program (ACMAP), and the NASA Modeling, Analysis, and Prediction (MAP). DCA also received support from the NASA Upper Atmospheric Research Program under NNH12ZDA001N-UACO. JMN was also supported by the NASA Postdoctoral Program at the NASA Goddard Space Flight Center, administered by Universities Space Research Association under contract with NASA. CONTRAST was funded by the NSF, and CONTRAST data are publicly available at 'http://data.eol.ucar.edu/ master_list/?project=CONTRAST'. ATTREX was funded by NASA and ATTREX data are publicly available at 'https://espoarchive.nasa.gov/archive/browse/ attrex/id4/GHawk'. The National Center for Environmental Prediction (NCEP) meteorological data are available at 'https://doi.org/10.5065/ D6M043C6'.

CCMI outputs from CESM1-WACCM and CESM1-CAM4Chem outputs are archived by NCAR at 'www.earthsystemgrid.org'. All other CCMI RefC-2 simulations are archived by the British Atmospheric Data Centre at 'http://badc.nerc.ac.uk/'. Output from CAM-chem-SD, TOMCAT, and EMAC-L90MA-SD are available upon request to pwales@umd.edu. The TOMCAT modelling was supported by NERC NCAS and the simulations were performed on the Archer and Leeds HPC Systems. CCSRNIES' research was supported by the Environment Research and Technology Development Fund (2-1303 and 2-1709) of the Ministry of the Environment, Japan, and computations were performed on NEC-SX9/A(ECO) computers at the CGER, NIES. RS and KAS, with ACCESS-CCM, acknowledge support from Australian Research Council's Centre of Excellence for Climate System Science (CE110001028), the Australian Government's National Computational Merit Allocation Scheme (q90) and Australian Antarctic science grant program (FoRCES 4012).

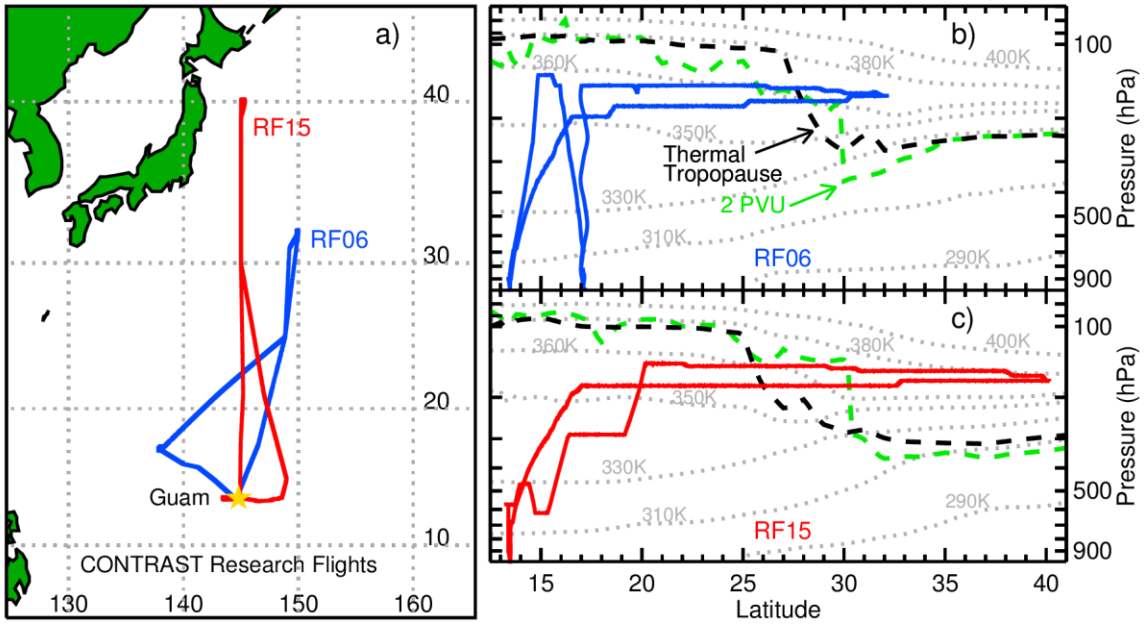

Figure 1. Flight paths for the only two CONTRAST research flights that reached the stratosphere, RF06 and RF15, are shown in panel (a). These flights were based out of Guam, indicated with a yellow star. The average potential temperatures, 2 PVU surface, and tropopause pressure from NCEP-FNL, sampled along the flight tracks, are shown for (b) RF06 (24 January 2014) and (c) RF15 (24 February 2014).

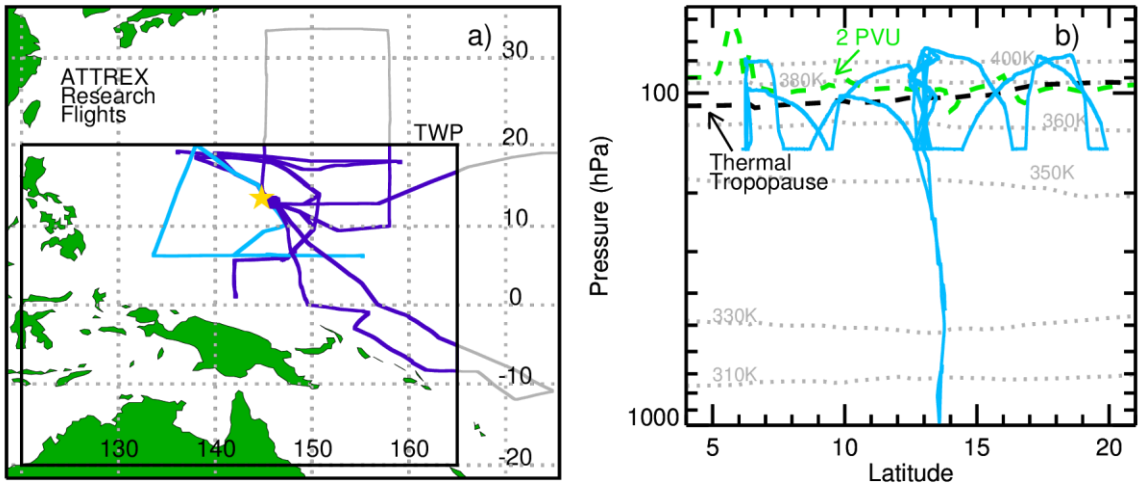

Figure 2. Flight paths of ATTREX 2014 research flights, based out of Guam (yellow star). (a) Flight tracks are shown as blue within the TWP (black box) and grey outside of the TWP. A sample ATTREX research flight, RF04, is highlighted in light blue. (b) RF04 sampled the stratosphere "vertically" within the tropics on 06 March 2014. Potential temperatures, the 2 PVU surface, and tropopause pressure are shown based on averaged NCEP-FNL analysis, sampled along RF04.

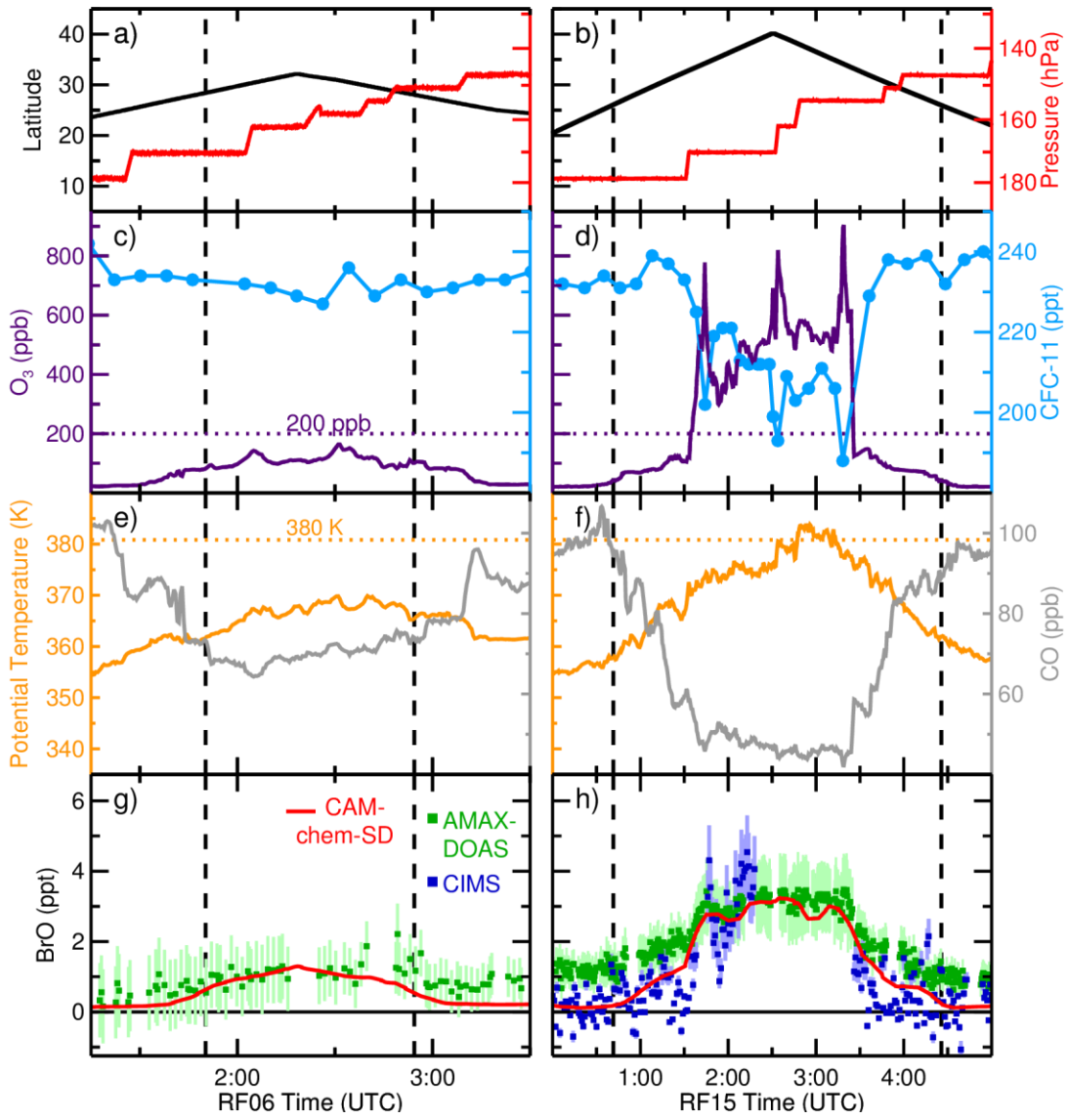

Figure 3. Time series for CONTRAST RF06 (left panels) and RF15 (right panels). The black dashed vertical lines indicate when the plane crossed the NCEP-FNL **thermal** tropopause. (a and b) The Gulfstream V (GV) aircraft latitude and **pressure**, (c and d) chemiluminescence O_3 and AWAS CFC-11 (e and f), as well as potential temperature and VUV CO are shown. (g and h) AMAX-DOAS and CIMS observed BrO and CAM-chem-SD modeled BrO are shown. Light green and blue bars indicate reported uncertainty in AMAX-DOAS and CIMS BrO, respectively. CIMS BrO is only available for RF15 when mixing ratios of O_3 are below 480 ppb (**see Section 2.1.1**).

1191

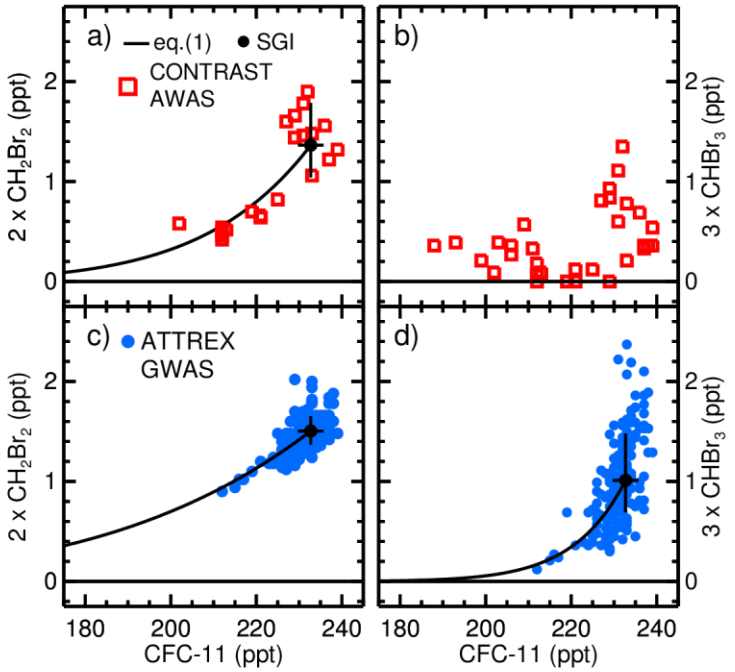

1192

1193 **Figure 4.** Stratospheric WAS observations of VSLS as function of CFC-11. The solid lines are
1194 the linear fit to the WAS observations (equation 2). The black points are SGI of each compound,
1195 calculated from equation (2). The horizontal error bars are the standard deviation in the mean
1196 measurements of CFC-11 at 17 km, and the vertical error bars are the uncertainty in the fit where
1197 CFC-11 is 233 ppt. (a) CONTRAST AWAS measurements CH_2Br_2 and CFC-11, collected in the
1198 extratropical stratosphere, are shown. (b) Poor relations between CONTRAST AWAS
1199 measurements of $CHBr_3$ and CFC-11 prevented the calculation of a meaningful fit. Stratospheric
1200 ATTREX GWAS observations of (c) CH_2Br_2 and (d) $CHBr_3$ as a function of CFC-11 are shown
1201 for the TWP.

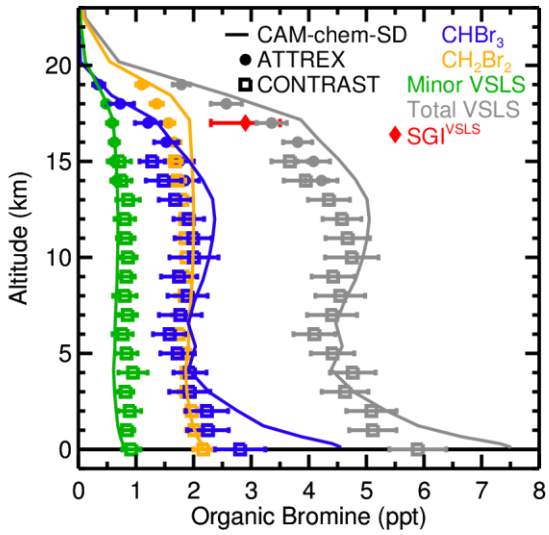

Figure 5. Profiles of VSLS in the TWP. WAS observations are sorted into 1 km bins. Square points are CONTRAST AWAS means, circle points are ATTREX GWAS means, and error bars are the standard deviation of each bin. The solid lines are average CAM-chem-SD profiles in the TWP. Minor VSLS (green) is the sum of CH_2BrCl, $CHBr_2Cl$, and $CHBrCl_2$, and total VSLS (grey) is the sum of minor VSLS, $CHBr_3$, and CH_2Br_2. The red diamond is SGI^{VSLS} calculated from CFC-11 tracer relations, 2.9 ± 0.6 ppt (Table 2). In all cases, mixing ratios of the VSLS are multiplied by bromine atomicity.

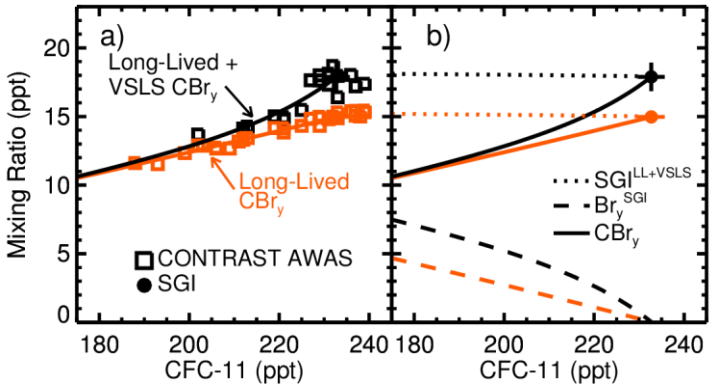

Figure 6. Tracer relations between bromine and CFC-11. In both panels orange lines and points are the sum of bromine supplied by only long-lived compounds, and black lines and points are the sum of bromine supplied by long-lived compounds and VSLS. Circle points and error bars are the mean and standard deviation of CBr_y and CFC-11 at the base of the stratosphere (where CFC-11 is 233 ppt). (a) The solid lines are the calculated tracer relations between CBr_y and CFC-11 from CONTRAST and ATTREX stratospheric observations (Table 2). Squares represent the sum of CONTRAST AWAS stratospheric measurements of bromocarbons collected during RF06 and RF15. (b) Br_y^{SGI} (dashed lines) calculated from the difference between CBr_y (solid lines) and $SGI^{LL+VSLS}$ (dotted lines) calculated according to equation (4) are shown.

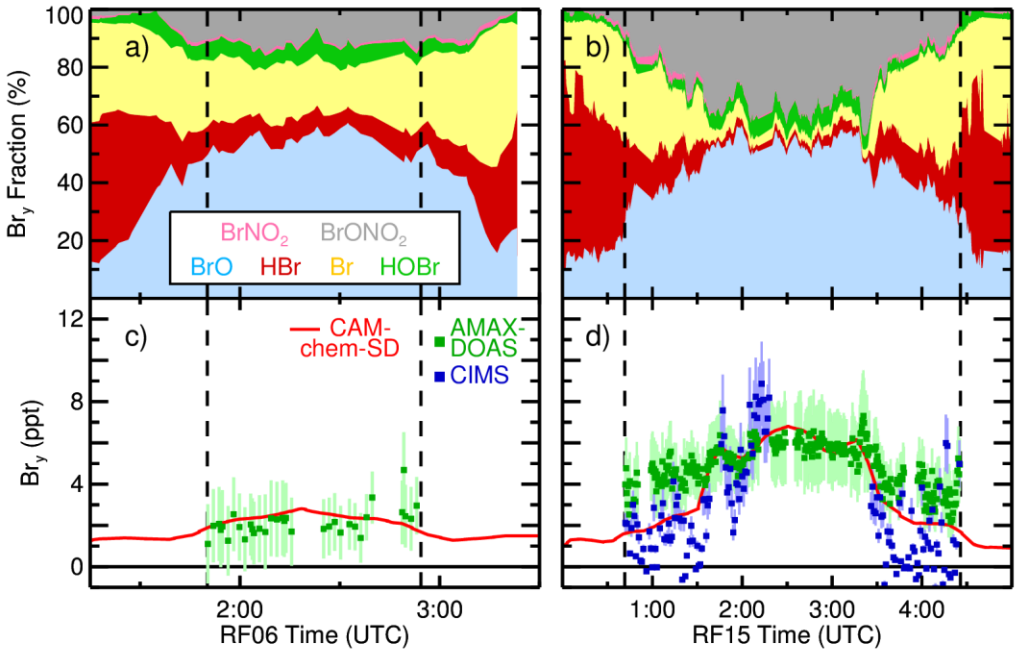

Figure 7. Model output and inferred Br_y for CONTRAST RF06 (left) and RF15 (right). In all panels, black vertical dashed lines indicate when the plane crossed the tropopause. (top panels) Br_y partitioning within the box model is shown. (bottom panels) Br_y inferred using the box modeled BrO/Br_y ratio as well as AMAX-DOAS (green) and CIMS (blue) BrO observations (Figure 3). Error bars are the modeled BrO/Br_y ratio applied to BrO measurement uncertainties. Red lines are CAM-chem-SD modeled Br_y interpolated to the flight track.

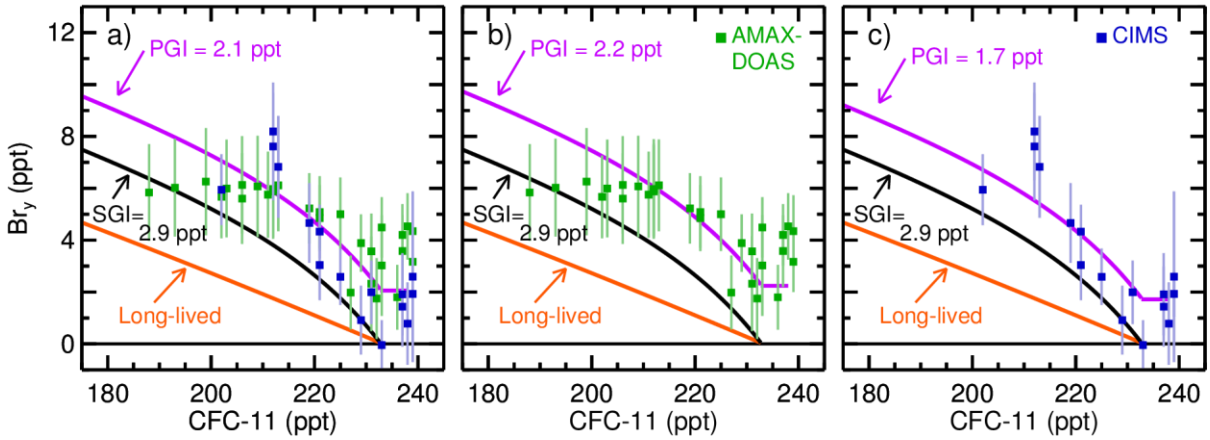

Figure 8. Modeled Br_y, inferred from observations of BrO, are shown as a function of observed CFC-11. In all panels square points are Br_y inferred from DOAS (green) and CIMS (blue) measurements of BrO, averaged for 5 minutes at the time of stratospheric AWAS measurements of CFC-11. Orange and black lines are Br_y^{SGI} for long-lived and the sum of long-lived and VSLS, respectively (dashed lines in Figure 6b). Purple lines are Br_y^{SGI} + PGI (a) The mean and standard deviation of PGI estimated using both AMAX-DOAS and CIMS-inferred Br_y is 2.1 ± 1.3 ppt. (b) PGI estimated using only AMAX-DOAS inferred Br_y is 2.2 ± 1.3 ppt. (c) PGI estimated using only CIMS-inferred Br_y is 1.7 ± 1.3 ppt.

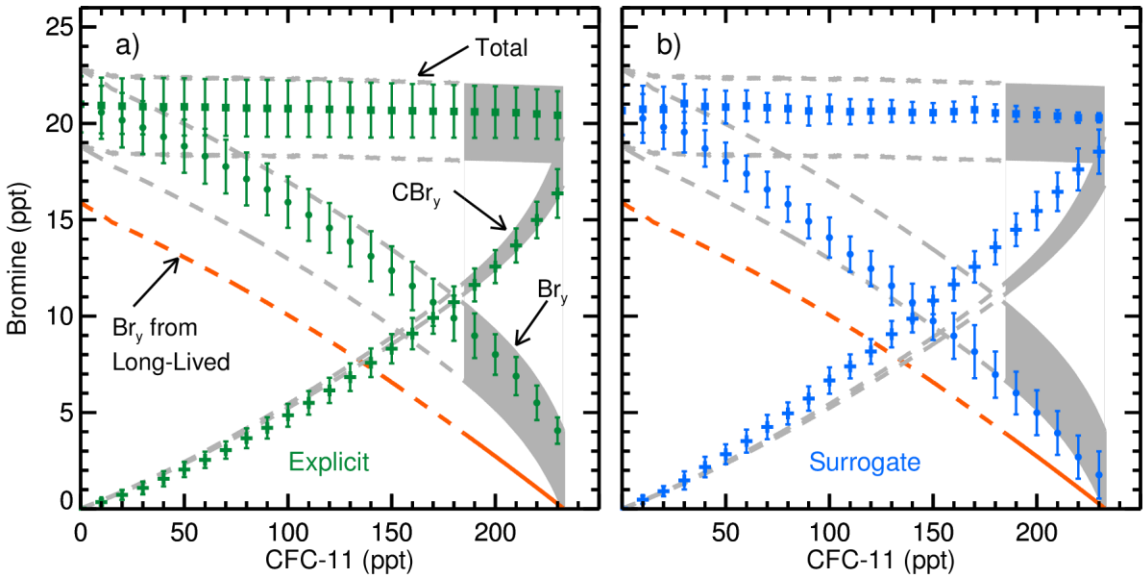

Figure 9. Observed and modeled relations of bromine as a function of CFC-11. Relations of CBr_y, Br_y, and total bromine as a function of CFC-11, calculated from observations, are shown in grey. Orange lines represent the expected rise of Br_y from the stratospheric supply of long-lived compounds only, calculated using measurements of CH_3Br and halons (orange, dashed line in Figure 6b). Shaded grey regions represent the range of uncertainty in the observed relation, and dashed grey lines represent extrapolations of the observed relations beyond the range of measured CFC-11. The observed CBr_y relation includes 2.9 ± 0.6 ppt from SGI^{VSLS} and the limits of this relation are defined according to the uncertainty in the linear fit of equation (2). The limits of both observed Br_y and total bromine relations are defined according to the 0.0 to 4.2 ppt range in observed PGI. **Points and error bars are the multi-model mean and standard deviation of (a) CCMI models with explicit and (b) surrogate representations of VSLS.** Model output is filtered for north of 30°N and binned for every 10 ppt of CFC-11.

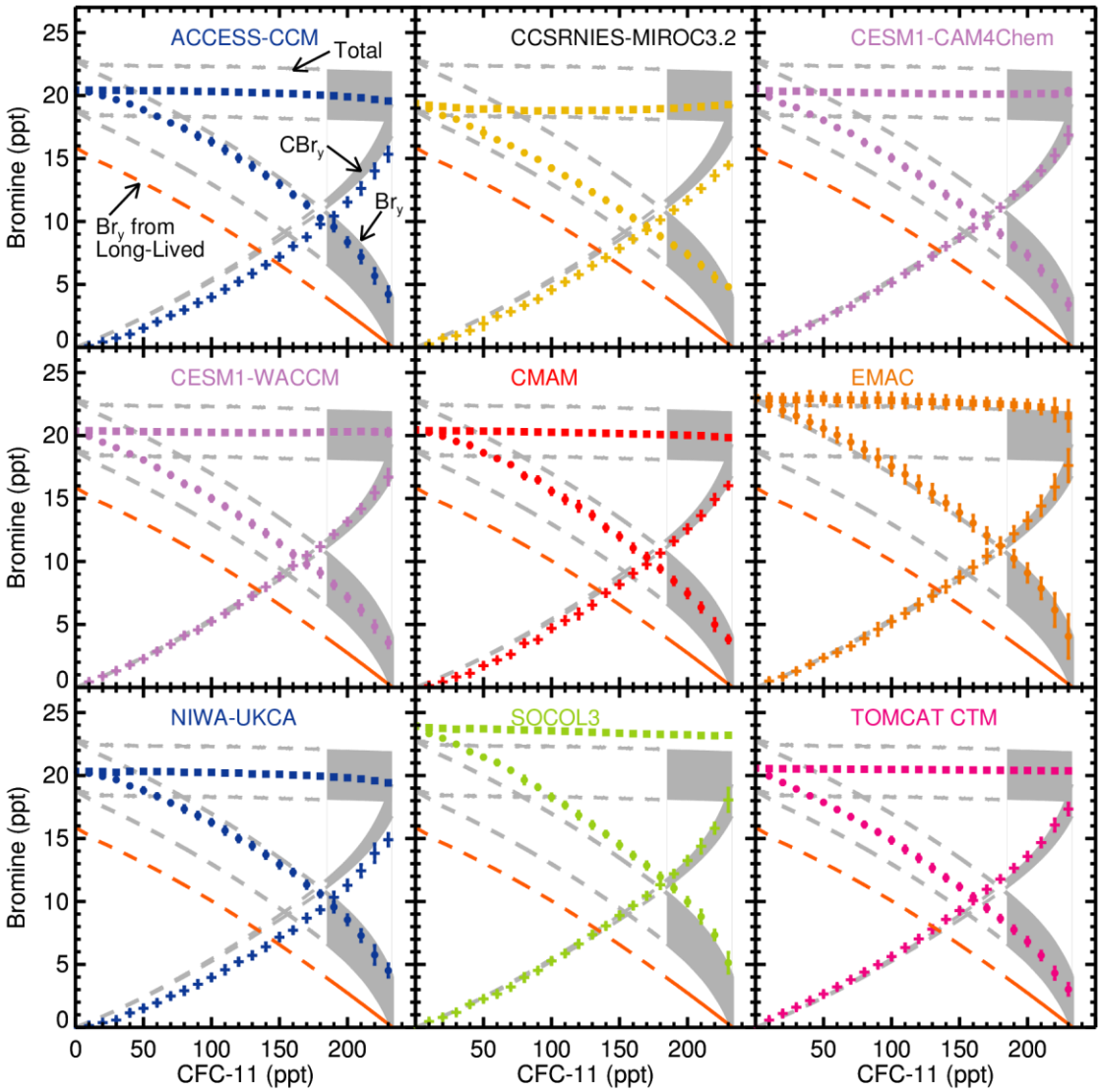

Figure 10. Same as Figure 9, but for individual CCMI models with explicit representations of VSLS. **The mean of three simulations, shown in Figure S11, is used for EMAC.**

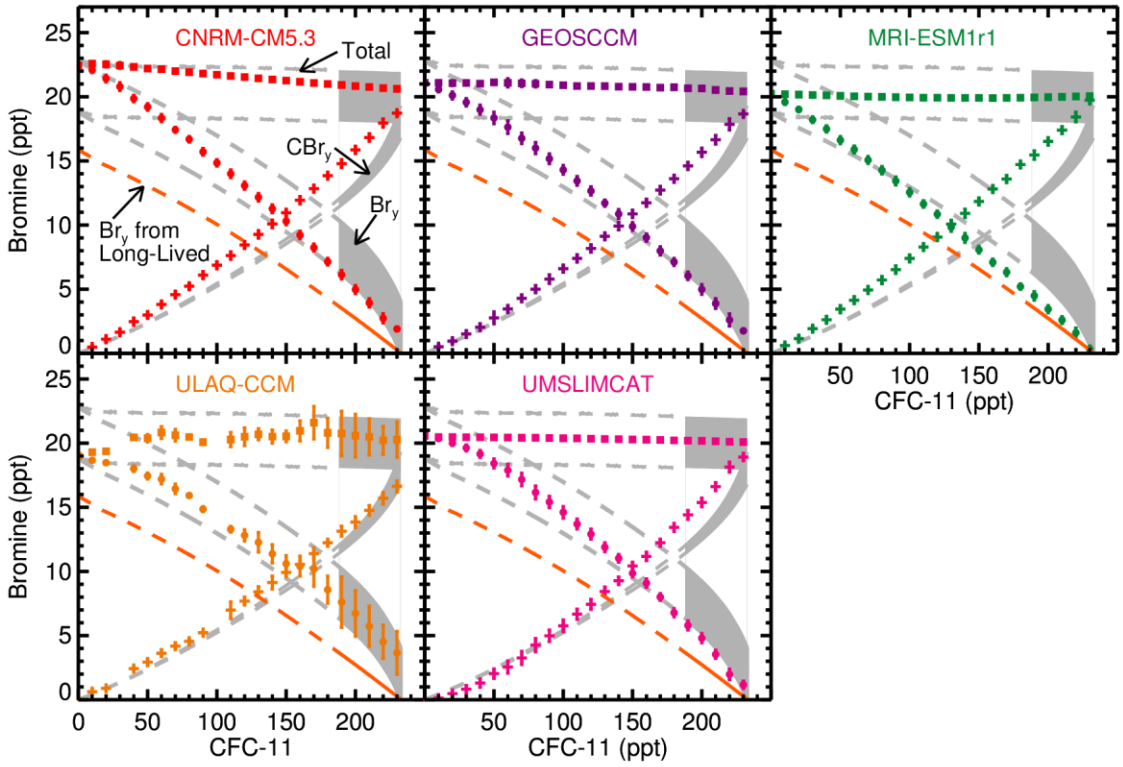

Figure 11. Same as Figure 9, but for individual CCMI models with surrogate representations of VSLS.

1258 **Table 1**. The GV HIAPER measurements, collected during CONTRAST RF06 and RF15, used
1259 to constrain the steady-state box model.

Instrument	Measurement	**Reference**
Airborne Multiaxis DOAS (AMAX-DOAS)	NO_2 (NO_y)	Koenig et al. (2017)
Advanced Whole Air Sampler (AWAS)	CFC-11 (Cl_y)	Schauffler et al. (2003)
Chemiluminescence	O_3	Ridley & Grahek (1990)
HIAPER Airborne Radiation Package (HARP)	$J(NO_2)$ and $J(O_3 \rightarrow O(^1D))$	Shetter & Müller (1999)
Picarro	CH_4	Crosson (2008)
Open Path Hygrometer	H_2O	Zondlo et al. (2010)
Ultra-High Sensitivity Aerosol Spectrometer (UHSAS)	Aerosol surface area density	Cai et al. (2008)
AeroLaser vacuum ultraviolet (VUV)	CO	Gerbig et al. (1999)

1260

1261 **Table 2.** Fitting parameters for the stratospheric tracer-tracer relation between bromocarbons and
1262 CFC-11 (equation 1).

	CBr_y	WMO lifetime[a]	$(X)_o$ (ppt)	d	Source
Long-lived	CH_3Br	26.3 years	7.20 ± 0.21	0.77 ± 0.09	CONTRAST
	$CBrClF_2$ (halon-1211)	41	3.72 ± 0.09	0.66 ± 0.06	CONTRAST
	$CBrF_3$ (halon-1301)	73.5	3.24 ± 0.06	1.265 ± 0.001	CAM-chem-SD
	$C_2Br_2F_4$ (halon-2402)	41	0.81 ± 0.03	0.73 ± 0.08	CONTRAST
	SGI^{LL}		15.0 ± 0.2		
VSLS	CH_2Br_2	150 days	1.36 ± 0.42	0.10 ± 0.03	CONTRAST
	$CHBr_3$	17	1.01 ± 0.47	0.05 ± 0.01	ATTREX
	$CHBrCl_2$	48	0.24 ± 0.07	0.06 ± 0.01	ATTREX[b]
	$CHBr_2Cl$	28	0.20 ± 0.08	0.06 ± 0.01	ATTREX
	CH_2BrCl	174	0.11 ± 0.03	0.12 ± 0.03	CONTRAST
	SGI^{VSLS}		2.9 ± 0.6		

1263 *Note:* All mixing ratios are multiplied by the bromine atomicity.
1264 [a]The WMO 2014 lifetimes are the stratospheric partial lifetime for long-lived compounds and the
1265 10 km tropical lifetime for VSLS.
1266 [b]For $CHBrCl_2$ $(X)_o$ is the ATTREX TWP mean at 17 km and d from $CHBr_2Cl$ is used.

1267 **Table 3.** Mean mixing ratios between 16.5 and 17.5 km from ATTREX and WMO 2014.

VSLS	ATTREX TWP 17 km mean (ppt)	WMO 2014 Tropical 17 km mean (ppt)
CH_2Br_2	1.56 ± 0.10	1.06 (0.6 – 1.72)
$CHBr_3$	1.21 ± 0.23	0.24 (0.00 – 0.93)
$CHBrCl_2$	0.24 ± 0.07	0.06 (0.03 – 0.12)
$CHBr_2Cl$	0.22 ± 0.05	0.04 (0.00 – 0.28)
CH_2BrCl	0.12 ± 0.02	0.07 (0.05 – 0.11)
SGI^{VSLS}	3.4 ± 0.3	1.4 (0.7 – 3.4)

1268 *Note:* All mixing ratios are multiplied by the bromine atomicity.

1269

1270 **Table 4. The bromine sources included in CCMI models considered by our study.**

Model	Bromine sources	References
ACCESS-CCM	CH_3Br, $CHBr_3$, CH_2Br_2	Stone et al. (2016)
CCSRNIES	CH_3Br, halons, $CHBr_3$, CH_2Br_2	Akiyoshi et al. (2016)
CESM1 CAM4-Chem	CH_3Br, halons, $CHBr_3$, CH_2Br_2	Lamarque et al. (2012); Tilmes et al. (2016)
CESM1 WACCM	CH_3Br, halons, $CHBr_3$, CH_2Br_2	Garcia et al. (2017); Marsh et al. (2013); Solomon et al. (2015)
CMAM	CH_3Br, $CHBr_3$, CH_2Br_2	Scinocca et al. (2008)
EMAC	CH_3Br, halons, $CHBr_3$, CH_2Br_2, minor VSLS, sea salt	Jöckel et al. (2016); Kerkweg et al. (2008)
NIWA-UKCA	CH_3Br, $CHBr_3$, CH_2Br_2	Morgenstern et al. (2009)
SOCOL3	CH_3Br, halons, $CHBr_3$, CH_2Br_2	Stenke et al. (2013)
TOMCAT CTM	CH_3Br, halons, $CHBr_3$, CH_2Br_2	Chipperfield (2006)
CNRM-CM5.3	CH_3Br (+5ppt), halons	Michou et al. (2011); Voldoire et al. (2012)
GEOSCCM	CH_3Br (+5ppt), halons	Oman et al. (2013)
MRI-ESM1	CH_3Br (+5ppt), halons	Deushi & Shibata (2011); Yukimoto et al. (2012)
ULAQ-CCM	CH_3Br (+5ppt), halons	Pitari et al. (2014)
UMSLIMCAT	CH_3Br (+5ppt), halons	Tian & Chipperfield (2005)

1271
1272

Table 5. Stratospheric supply of bromine for winter 2014 from observations and CCMI models.

Source	SGI^{LL} (ppt)	SGI^{VSLS} (ppt)	PGI (ppt)	Total (ppt)
Observed	**15.0 ± 0.2**	**2.9 ± 0.6**	**2.1 ± 2.1**	**20.0 ± 2.1**
ACCESS-CCM	13.7 ± 0.2	2.0 ± 0.1	3.7 ± 0.3	19.4 ± 0.05
CCSRNIES-MIROC3.2	12.9 ± 0.05	2.0 ± 0.05	4.4 ± 0.2	19.3 ± 0.03
CESM1 CAM4-chem	14.2 ± 0.2	2.2 ± 0.07	3.0 ± 0.4	19.3 ± 0.06
CESM1 WACCM	14.4 ± 0.2	2.3 ± 0.08	2.9 ± 0.4	19.6 ± 0.1
CMAM	14.0 ± 0.1	2.8 ± 0.09	3.1 ± 0.3	19.9 ± 0.02
EMAC-L47MA	12.9 ± 0.2	5.0 ± 0.3	4.8 ± 0.8	22.7 ± 0.5
EMAC-L90MA	13.1 ± 0.1	5.1 ± 0.2	4.6 ± 0.5	22.8 ± 0.5
EMAC-L90MA-SD	13.5 ± 0.2	5.7 ± 2.3	3.7 ± 0.8	22.9 ± 0.8
NIWA-UKCA	13.5 ± 0.1	1.9 ± 0.1	3.8 ± 0.3	19.2 ± 0.07
SOCOL3	14.4 ± 0.1	3.0 ± 0.2	5.3 ± 0.5	22.7 ± 0.02
TOMCAT CTM	14.6 ± 0.8	3.4 ± 0.9	2.3 ± 1.6	20.4 ± 0.02
Explicit models	**13.9 ± 0.6**	**2.8 ± 1.1**	**3.6 ± 0.9**	**20.3 ± 1.5**
CNRM-CM5.3	19.6 ± 0.1		0.9 ± 0.2	20.5 ± 0.01
GEOSCCM	19.5 ± 0.06		1.2 ± 0.2	20.7 ± 0.1
MRI-ESM1r1	19.4 ± 0.01		0.7 ± 0.01	20.0 ± 0.07
ULAQ-CCM	17.0 ± 0.2		1.3 ± 0.3	18.4 ± 0.2
UMSLIMCAT	19.6 ± 0.08		0.7 ± 0.1	20.3 ± 0.1
Surrogate models	**19.0 ± 1.1**		**1.0 ± 0.3**	**20.0 ± 1.0**

Note: First row shows observed values from Table 2. Other entries are based on model output at the tropical tropopause pressure for January to March 2014.

References

Akiyoshi, H., Nakamura, T., Miyasaka, T., Shiotani, M., & Suzuki, M. (2016). A nudged chemistry-climate model simulation of chemical constituent distribution at northern high-latitude stratosphere observed by SMILES and MLS during the 2009/2010 stratospheric sudden warming. *Journal of Geophysical Research: Atmospheres*, *121*(3), 1361–1380. https://doi.org/10.1002/2015JD023334

Anderson, D. C., Nicely, J. M., Salawitch, R. J., Canty, T. P., Dickerson, R. R., Hanisco, T. F., … Weinheimer, A. J. (2016). A pervasive role for biomass burning in tropical high ozone/low water structures. *Nature Communications*, *7*(10267). https://doi.org/10.1038/ncomms10267

Andrews, S. J., Carpenter, L. J., Apel, E. C., Atlas, E., Donets, V., Hopkins, J. F., … Schauffler, S. (2016). A comparison of very short-lived halocarbon (VSLS) and DMS aircraft measurements in the Tropical West Pacific from CAST, ATTREX and CONTRAST. *Atmospheric Measurement Techniques Discussions*, *9*, 1–23. https://doi.org/10.5194/amt-2016-94

Aschmann, J., & Sinnhuber, B. M. (2013). Contribution of very short-lived substances to stratospheric bromine loading: Uncertainties and constraints. *Atmospheric Chemistry and Physics*, *13*(3), 1203–1219. https://doi.org/10.5194/acp-13-1203-2013

Aschmann, J., Sinnhuber, B. M., Atlas, E. L., & Schauffler, S. M. (2009). Modeling the transport of very short-lived substances into the tropical upper troposphere and lower stratosphere. *Atmospheric Chemistry and Physics*, *9*(23), 9237–9247. https://doi.org/10.5194/acp-9-9237-2009

Aschmann, J., Sinnhuber, B. M., Chipperfield, M. P., & Hossaini, R. (2011). Impact of deep convection and dehydration on bromine loading in the upper troposphere and lower stratosphere. *Atmospheric Chemistry and Physics*, *11*(6), 2671–2687. https://doi.org/10.5194/acp-11-2671-2011

Avallone, L. M., & Prather, M. J. (1997). Tracer-Tracer Correlations: Three-Dimensional Model Simulations and Comparisons to Observations. *J. Geophys. Res.*, *102*(D15), 19233–19246. https://doi.org/10.1029/2007JG000640/abstract

Baidar, S., Oetjen, H., Coburn, S., Dix, B., Ortega, I., Sinreich, R., & Volkamer, R. (2013). The CU Airborne MAX-DOAS instrument: vertical profiling of aerosol extinction and trace gases. *Atmospheric Measurement Techniques*, *6*(3), 719–739. https://doi.org/10.5194/amt-6-719-2013

Bergman, J. W., Jensen, E. J., Pfister, L., & Yang, Q. (2012). Seasonal differences of vertical-transport efficiency in the tropical tropopause layer: On the interplay between tropical deep convection, large-scale vertical ascent, and horizontal circulations. *Journal of Geophysical Research Atmospheres*, *117*(D05302), 1–20. https://doi.org/10.1029/2011JD016992

Brinckmann, S., Engel, A., Bönisch, H., Quack, B., & Atlas, E. (2012). Short-lived brominated hydrocarbons - Observations in the source regions and the tropical tropopause layer. *Atmospheric Chemistry and Physics*, *12*(3), 1213–1228. https://doi.org/10.5194/acp-12-1213-2012

Burkholder, J. B., Sander, S. P., Abbatt, J., Barker, J. R., Huie, R. E., Kolb, C. E., … Wine, P. H. (2015). *Chemical Kinetics and Photochemical Data for Use in Atmospheric Studies, Evaluation Number 18. JPL Publication 15-10*. Jet Propulsion Laboratory, Pasadena, Calif.: JPL Publication 15-10. Retrieved from http://jpldataeval.jpl.nasa.gov/

Cai, Y., Montague, D. C., Mooiweer-Bryan, W., & Deshler, T. (2008). Performance

characteristics of the ultra high sensitivity aerosol spectrometer for particles between 55 and 800 nm: Laboratory and field studies. *Journal of Aerosol Science*, *39*(9), 759–769. https://doi.org/10.1016/j.jaerosci.2008.04.007

Carpenter, L. J., & Liss, P. S. (2000). On temperate sources of bromoform and other reactive organic bromine gases. *Journal of Geophysical Research*, *105*(D16), 20539–20547. https://doi.org/10.1029/2000JD900242

Carpenter, L. J., Reimann, S., Burkholder, J. B., Clerbaux, C., Hall, B. D., Hossaini, R., … Yvon-Lewis, S. A. (2014). Ozone-Depleting Substances (ODSs) and Other Gases of Interest to the Montreal Protocol, Chapter 1. In *Scientific Assessment of Ozone Depletion: 2014, Global Ozone Research and Monitoring Project – Report No. 55*. Geneva, Switzerland: World Meteorological Organization.

Chen, D., Huey, L. G., Tanner, D. J., Salawitch, R. J., Anderson, D. C., Wales, P. A., … Wolfe, G. M. (2016). Airborne measurements of BrO and the sum of HOBr and Br2 over the Tropical West Pacific from 1 to 15 km during the CONvective TRansport of Active Species in the Tropics (CONTRAST) experiment. *J. Geophys. Res. Atmos.*, *121*, 1–19. https://doi.org/10.1002/2016JD025561

Chipperfield, M. P. (2006). New version of the TOMCAT/SLIMCAT off-line chemical transport model: Intercomparison of stratospheric tracer experiments. *Quarterly Journal of the Royal Meteorological Society*, *132*(617), 1179–1203. https://doi.org/10.1256/qj.05.51

Choi, S., Wang, Y., Salawitch, R. J., Canty, T., Joiner, J., Zeng, T., … Levelt, P. F. (2012). Analysis of satellite-derived Arctic tropospheric BrO columns in conjunction with aircraft measurements during ARCTAS and ARCPAC. *Atmospheric Chemistry and Physics*, *12*(3), 1255–1285. https://doi.org/10.5194/acp-12-1255-2012

Crosson, E. R. (2008). A cavity ring-down analyzer for measuring atmospheric levels of methane, carbon dioxide, and water vapor. *Applied Physics B*, *92*(3), 403–408. https://doi.org/10.1007/s00340-008-3135-y

Deushi, M., & Shibata, K. (2011). Development of a Meteorological Research Institute chemistry-climate model version 2 for the study of tropospheric and stratospheric chemistry. *Papers in Meteorology and Geophysics*, *62*(May), 1–46. https://doi.org/10.2467/mripapers.62.1

Dix, B., Koenig, T. K., & Volkamer, R. (2016). Parameterization retrieval of trace gas volume mixing ratios from Airborne MAX-DOAS. *Atmospheric Measurement Techniques*, *9*(11), 5655–5675. https://doi.org/10.5194/amt-9-5655-2016

Dorf, M., Butler, J. H., Butz, A., Camy-Peyret, C., Chipperfield, M. P., Kritten, L., … Pfeilsticker, K. (2006). Long-term observations of stratospheric bromine reveal slow down in growth. *Geophysical Research Letters*, *33*(24), L24803. https://doi.org/10.1029/2006GL027714

Dorf, M., Butz, A., Camy-Peyret, C., Chipperfield, M. P., Kritten, L., & Pfeilsticker, K. (2008). Bromine in the tropical troposphere and stratosphere as derived from balloon-borne BrO observations. *Atmospheric Chemistry and Physics Discussions*, *8*(4), 12999–13015. https://doi.org/10.5194/acpd-8-12999-2008

Douglass, A., Fioletov, V., Godin-Beekmann, S., Müller, R., Stolarski, R. S., & Webb, A. (2011). Stratospheric Ozone and Surface Ultraviolet Radiation. In *Scientific Assessment of Ozone Depletion* (52nd ed.). Geneva, Switzerland.

Dvortsov, V. L., Geller, M. A., Solomon, S., Schauffler, S. M., Atlas, E. L., & Blake, D. R. (1999). Rethinking reactive halogen budgets in the midlatitude lower stratosphere.

Geophysical Research Letters, *26*(12), 1699–1702. https://doi.org/10.1029/1999GL900309

Engel, A., Strunk, M., Müller, M., Haase, H.-P., Poss, C., Levin, I., & Schmidt, U. (2002). Temporal development of total chlorine in the high-latitude stratosphere based on reference distributions of mean age derived from CO_2 and SF6. *J. Geophys. Res*, *107*(12), ACH 1-1-ACH 1-11. https://doi.org/10.1029/2001JD000584

Eyring, V., Lamarque, J.-F., Hess, P., Arfeuille, F., Bowman, K., Chipperfield, M. P., … Young, P. J. (2013). Overview of IGAC/SPARC Chemistry-Climate Model Initiative (CCMI) Community Simulations in Support of Upcoming Ozone and Climate Assessments. *SPARC Newsletter*, *40*(January), 48–66. https://doi.org/SPARC Newsletter No. 40, p. 48-66, 2013

Falk, S., Sinnhuber, B.-M., Krysztofiak, G., Jöckel, P., Graf, P., & Lennartz, S. T. (2017). Brominated VSLS and their influence on ozone under a changing climate. *Atmospheric Chemistry and Physics*, *17*(18), 11313–11329. https://doi.org/10.5194/acp-17-11313-2017

Feng, W., Chipperfield, M. P., Dorf, M., Pfeilsticker, K., & Ricaud, P. (2007). Mid-latitude ozone changes: studies with a 3-D CTM forced by ERA-40 analyses. *Atmospheric Chemistry and Physics*, *7*(9), 2357–2369. https://doi.org/10.5194/acp-7-2357-2007

Fernandez, R. P., Kinnison, D. E., Lamarque, J.-F., Tilmes, S., & Saiz-Lopez, A. (2017). Impact of biogenic very short-lived bromine on the Antarctic ozone hole during the 21st century. *Atmospheric Chemistry and Physics*, *17*(3), 1673–1688. https://doi.org/10.5194/acp-17-1673-2017

Fernandez, R. P., Salawitch, R. J., Kinnison, D. E., Lamarque, J. F., & Saiz-Lopez, A. (2014). Bromine partitioning in the tropical tropopause layer: Implications for stratospheric injection. *Atmospheric Chemistry and Physics*, *14*(24), 13391–13410. https://doi.org/10.5194/acp-14-13391-2014

Garcia, R. R., Smith, A. K., Kinnison, D. E., Cámara, Á. de la, & Murphy, D. J. (2017). Modification of the Gravity Wave Parameterization in the Whole Atmosphere Community Climate Model: Motivation and Results. *Journal of the Atmospheric Sciences*, *74*(1), 275–291. https://doi.org/10.1175/JAS-D-16-0104.1

Gerbig, C., Schmitgen, S., Kley, D., Volz-Thomas, A., Dewey, K., & Haaks, D. (1999). An improved fast-response vacuum-UV resonance fluorescence CO instrument. *Journal of Geophysical Research: Atmospheres*, *104*(D1), 1699–1704. https://doi.org/10.1029/1998JD100031

Gettelman, A., Hoor, P., Pan, L. L., Randel, W. J., Hegglin, M. I., & Birner, T. (2011). The Extratropical Upper Troposphere and Lower Stratosphere. *Reviews of Geophysics*, *49*(3), RG3003. https://doi.org/10.1029/2011RG000355

Hall, T. M., & Plumb, R. A. (1994). Age as a diagnostic of stratospheric transport. *Journal of Geophysical Research*, *99*(D1), 1059–1070. https://doi.org/10.1029/93JD03192

Harris, N. R. P., Carpenter, L. J., Lee, J. D., Vaughan, G., Filus, M. T., Jones, R. L., … Manning, A. J. (2017). Coordinated Airborne Studies in the Tropics (CAST). *Bulletin of the American Meteorological Society*, *98*(1), 145–162. https://doi.org/10.1175/BAMS-D-14-00290.1

Harris, N. R. P., Wuebbles, D. J., Daniel, J. S., Hu, J., Kuijpers, L. J. M., Law, K. S., … Schofield, R. (2014). Chapter 5: Scenarios and Information for Policymakers. *Scientific Assessment of Ozone Depletion: 2014, Global Ozone Research and Monitoring Project – Report No. 55*,.

Holton, J. R., Haynes, P. H., McIntyre, M. E., Douglass, A. R., Rood, R. B., & Pfister, L. (1995). Stratosphere-troposphere exchange. *Reviews of Geophysics*, *33*(4), 403–439. https://doi.org/10.1029/95RG02097

1414 Hossaini, R., Chipperfield, M. P., Feng, W., Breider, T. J., Atlas, E., Montzka, S. A., … Elkins,
1415 J. (2012). The contribution of natural and anthropogenic very short-lived species to
1416 stratospheric bromine. *Atmospheric Chemistry and Physics*, *12*(1), 371–380.
1417 https://doi.org/10.5194/acp-12-371-2012
1418 Hossaini, R., Chipperfield, M. P., Monge-Sanz, B. M., Richards, N. a. D., Atlas, E., & Blake, D.
1419 R. (2010). Bromoform and dibromomethane in the tropics: a 3-D model study of chemistry
1420 and transport. *Atmospheric Chemistry and Physics*, *10*(2), 719–735.
1421 https://doi.org/10.5194/acp-10-719-2010
1422 Hossaini, R., Mantle, H., Chipperfield, M. P., Montzka, S. A., Hamer, P., Ziska, F., …
1423 Pfeilsticker, K. (2013). Evaluating global emission inventories of biogenic bromocarbons.
1424 *Atmospheric Chemistry and Physics*, *13*(23), 11819–11838. https://doi.org/10.5194/acp-13-
1425 11819-2013
1426 Hossaini, R., Patra, P. K., Leeson, A. A., Krysztofiak, G., Abraham, N. L., Andrews, S. J., …
1427 Ziska, F. (2016). A multi-model intercomparison of halogenated very short-lived substances
1428 (TransCom-VSLS): Linking oceanic emissions and tropospheric transport for a reconciled
1429 estimate of the stratospheric source gas injection of bromine. *Atmospheric Chemistry and*
1430 *Physics*, *16*(14), 9163–9187. https://doi.org/10.5194/acp-16-9163-2016
1431 Huey, L. G. (2007). Measurement of trace atmospheric species by chemical ionization mass
1432 spectrometry: Speciation of reactive nitrogen and future directions. *Mass Spectrometry*
1433 *Reviews*, *26*(2), 166–184. https://doi.org/10.1002/mas.20118
1434 Jensen, E. J., Pfister, L., Jordan, D. E., Bui, T. V., Ueyama, R., Singh, H. B., … Pfeilsticker, K.
1435 (2017). The NASA Airborne Tropical Tropopause Experiment: High-Altitude Aircraft
1436 Measurements in the Tropical Western Pacific. *Bulletin of the American Meteorological*
1437 *Society*, *98*(1), 129–143. https://doi.org/10.1175/BAMS-D-14-00263.1
1438 Jöckel, P., Tost, H., Pozzer, A., Kunze, M., Kirner, O., Brenninkmeijer, C. A. M., … Zahn, A.
1439 (2016). Earth System Chemistry integrated Modelling (ESCiMo) with the Modular Earth
1440 Submodel System (MESSy) version 2.51. *Geoscientific Model Development*, *9*(3), 1153–
1441 1200. https://doi.org/10.5194/gmd-9-1153-2016
1442 Kerkweg, A., Jöckel, P., Warwick, N., Gebhardt, S., Brenninkmeijer, C. A. M., & Lelieveld, J.
1443 (2008). Consistent simulation of bromine chemistry from the marine boundary layer to the
1444 stratosphere – Part 2: Bromocarbons. *Atmospheric Chemistry and Physics*, *8*(19), 5919–
1445 5939. https://doi.org/10.5194/acp-8-5919-2008
1446 Klobas, J. E., Wilmouth, D. M., Weisenstein, D. K., Anderson, J. G., & Salawitch, R. J. (2017).
1447 Ozone depletion following future volcanic eruptions. *Geophysical Research Letters*.
1448 https://doi.org/10.1002/2017GL073972
1449 Ko, M. K. W., Poulet, G., Blake, D. R., Boucher, O., Burkholder, J. H., Chin, M., … Yokouchi,
1450 Y. (2003). Very Short-Lived Halogen and Sulfur Substances. In *Scientific Assessment of*
1451 *Ozone Depletion: 2002, Global Ozone Research and Monitoring Project* (47th ed.).
1452 Geneva, Switzerland.
1453 Ko, M. K. W., Sze, N., Scott, C. J., & Weisenstein, D. K. (1997). On the relation between
1454 stratospheric chlorine/bromine loading and short-lived tropospheric source gases. *Journal of*
1455 *Geophsyical Research*, *102*(D12), 25,507-25,517.
1456 Koenig, T. K., Volkamer, R., Baidar, S., Dix, B., Wang, S., Anderson, D. C., … Wolfe, G. M.
1457 (2017). BrO and inferred Bry profiles over the western Pacific: relevance of inorganic
1458 bromine sources and a Bry minimum in the aged tropical tropopause layer. *Atmospheric*
1459 *Chemistry and Physics*, *17*(24), 15245–15270. https://doi.org/10.5194/acp-17-15245-2017

Kovalenko, L. J., Livesey, N. L., Salawitch, R. J., Camy-Peyret, C., Chipperfield, M. P., Cofield, R. E., … Waters, J. W. (2007). Validation of Aura Microwave Limb Sounder BrO observations in the stratosphere. *Journal of Geophysical Research Atmospheres*, *112*(24), 1–17. https://doi.org/10.1029/2007JD008817

Kreycy, S., Camy-Peyret, C., Chipperfield, M. P., Dorf, M., Feng, W., Hossaini, R., … Pfeilsticker, K. (2013). Atmospheric test of the J($BrONO_2$)/$k_{BrO+NO2}$ ratio: implications for total stratospheric Br_y and bromine-mediated ozone loss. *Atmospheric Chemistry and Physics*, *13*(13), 6263–6274. https://doi.org/10.5194/acp-13-6263-2013

Lamarque, J.-F., Emmons, L. K., Hess, P. G., Kinnison, D. E., Tilmes, S., Vitt, F., … Tyndall, G. K. (2012). CAM-chem: description and evaluation of interactive atmospheric chemistry in the Community Earth System Model. *Geoscientific Model Development*, *5*(2), 369–411. https://doi.org/10.5194/gmd-5-369-2012

Laube, J. C., Engel, A., Bönisch, H., Möbius, T., Worton, D. R., Sturges, W. T., … Schmidt, U. (2008). Contribution of very short-lived organic substances to stratospheric chlorine and bromine in the tropics -- a case study. *Atmospheric Chemistry and Physics Discussions*, *8*(3), 8491–8515. https://doi.org/10.5194/acpd-8-8491-2008

Le Breton, M., Bannan, T. J., Shallcross, D. E., Khan, M. A., Evans, M. J., Lee, J., … Percival, C. J. (2017). Enhanced ozone loss by active inorganic bromine chemistry in the tropical troposphere. *Atmospheric Environment*, *155*, 21–28. https://doi.org/10.1016/j.atmosenv.2017.02.003

Lennartz, S. T., Krysztofiak, G., Marandino, C. A., Sinnhuber, B. M., Tegtmeier, S., Ziska, F., … Quack, B. (2015). Modelling marine emissions and atmospheric distributions of halocarbons and dimethyl sulfide: The influence of prescribed water concentration vs. prescribed emissions. *Atmospheric Chemistry and Physics*, *15*(20), 11753–11772. https://doi.org/10.5194/acp-15-11753-2015

Levine, J. G., Braesicke, P., Harris, N. R. P., Savage, N. H., & Pyle, J. A. (2007). Pathways and timescales for troposphere-to-stratosphere transport via the tropical tropopause layer and their relevance for very short lived substances. *Journal of Geophysical Research Atmospheres*, *112*(4), 1–15. https://doi.org/10.1029/2005JD006940

Liang, Q., Atlas, E., Blake, D., Dorf, M., Pfeilsticker, K., & Schauffler, S. (2014). Convective transport of very short lived bromocarbons to the stratosphere. *Atmospheric Chemistry and Physics*, *14*(11), 5781–5792. https://doi.org/10.5194/acp-14-5781-2014

Liang, Q., Stolarski, R. S., Kawa, S. R., Nielsen, J. E., Douglass, A. R., Rodriguez, J. M., … Ott, L. E. (2010). Finding the missing stratospheric Br_y: a global modeling study of $CHBr_3$ and CH_2Br_2. *Atmospheric Chemistry and Physics*, *10*(5), 2269–2286. https://doi.org/10.5194/acp-10-2269-2010

Liao, J., Sihler, H., Huey, L. G., Neuman, J. A., Tanner, D. J., Friess, U., … Ullmann, K. (2011). A comparison of Arctic BrO measurements by chemical ionization mass spectrometry and long path-differential optical absorption spectroscopy. *Journal of Geophysical Research Atmospheres*, *116*(1), 1–14. https://doi.org/10.1029/2010JD014788

Long, M. S., Keene, W. C., Easter, R. C., Sander, R., Liu, X., Kerkweg, A., & Erickson, D. (2014). Sensitivity of tropospheric chemical composition to halogen-radical chemistry using a fully coupled size-resolved multiphase chemistry-global climate system: Halogen distributions, aerosol composition, and sensitivity of climate-relevant gases. *Atmospheric Chemistry and Physics*, *14*(7), 3397–3425. https://doi.org/10.5194/acp-14-3397-2014

Marsh, D. R., Mills, M. J., Kinnison, D. E., Lamarque, J. F., Calvo, N., & Polvani, L. M. (2013).

Climate change from 1850 to 2005 simulated in CESM1(WACCM). *Journal of Climate*, *26*(19), 7372–7391. https://doi.org/10.1175/JCLI-D-12-00558.1

McLinden, C. A., Haley, C. S., Lloyd, N. D., Hendrick, F., Rozanov, A., Sinnhuber, B. M., … Burrows, J. P. (2010). Odin/OSIRIS observations of stratospheric BrO: Retrieval methodology, climatology, and inferred Br_y. *Journal of Geophysical Research Atmospheres*, *115*(15), 1–19. https://doi.org/10.1029/2009JD012488

Michou, M., Saint-Martin, D., Teyssèdre, H., Alias, A., Karcher, F., Olivié, D., … Chéroux, F. (2011). A new version of the CNRM Chemistry-Climate Model, CNRM-CCM: description and improvements from the CCMVal-2 simulations. *Geoscientific Model Development*, *4*(4), 873–900. https://doi.org/10.5194/gmd-4-873-2011

Mohd Nadzir, M. S., Phang, S. M., Abas, M. R., Abdul Rahman, N., Abu Samah, A., Sturges, W. T., … Hanafiah, M. M. (2014). Bromocarbons in the tropical coastal and open ocean atmosphere during the 2009 Prime Expedition Scientific Cruise (PESC-09). *Atmospheric Chemistry and Physics*, *14*(15), 8137–8148. https://doi.org/10.5194/acp-14-8137-2014

Molod, A., Takacs, L., Suarez, M., Bacmeister, J., Song, I., & Eichmann, A. (2012). *The GEOS-5 Atmospheric General Circulation Model : Mean Climate and Development from MERRA to Fortuna*. *Technical Report Series on Global Modeling and Data Assimilation* (Vol. 27).

Montzka, S. A., Reimann, S., Engel, A., Krüger, K., Sturges, W. T., & O'Doherty, S. (2011). Ozone-Depleting Substances (ODSs) and Related Chemicals. In *Scientific Assessment of Ozone Depletion: 2010, Global Ozone Research and Monitoring Project* (52nd ed.). Geneva, Switzerland.

Morgenstern, O., Akiyoshi, H., Yamashita, Y., Kinnison, D. E., Garcia, R. R., Plummer, D. A., … Chipperfield, M. P. (2017a). Ozone sensitivity to varying greenhouse gases and ozone-depleting substances in CCMI simulations. *Atmospheric Chemistry and Physics Discussions*, (July), 1–32. https://doi.org/10.5194/acp-2017-565

Morgenstern, O., Braesicke, P., O'Connor, F. M., Bushell, A. C., Johnson, C. E., Osprey, S. M., & Pyle, J. A. (2009). Evaluation of the new UKCA climate-composition model – Part 1: The stratosphere. *Geoscientific Model Development*, *2*(1), 43–57. https://doi.org/10.5194/gmd-2-43-2009

Morgenstern, O., Hegglin, M. I., Rozanov, E., O'Connor, F. M., Abraham, N. L., Akiyoshi, H., … Zeng, G. (2017b). Review of the global models used within phase 1 of the Chemistry–Climate Model Initiative (CCMI). *Geoscientific Model Development*, *10*(2), 639–671. https://doi.org/10.5194/gmd-10-639-2017

Navarro, M. A., Atlas, E. L., Saiz-Lopez, A., Rodriguez-Lloveras, X., Kinnison, D. E., Lamarque, J., … Donets, V. (2015). Airborne measurements of organic bromine compounds in the Pacific tropical tropopause layer. *Proceedings of the National Academy of Sciences*, *112*(45), 13789–13793. https://doi.org/10.1073/pnas.1511463112

Navarro, M. A., Saiz-Lopez, A., Cuevas, C. A., Fernandez, R. P., Atlas, E., Rodriguez-Lloveras, X., … Moore, F. L. (2017). Modeling the inorganic bromine partitioning in the tropical tropopause layer over the eastern and western Pacific Ocean. *Atmospheric Chemistry and Physics*, *17*(16), 9917–9930. https://doi.org/10.5194/acp-17-9917-2017

Nicely, J. M., Anderson, D. C., Canty, T. P., Salawitch, R. J., Wolfe, G. M., Apel, E. C., … Weinheimer, A. J. (2016). An observationally constrained evaluation of the oxidative capacity in the tropical western Pacific troposphere. *Journal of Geophysical Research: Atmospheres*, *121*(12), 7461–7488. https://doi.org/10.1002/2016JD025067

Oman, L. D., Douglass, A. R., Salawitch, R. J., Canty, T. P., Ziemke, J. R., & Manyin, M.

(2016). The effect of representing bromine from VSLS on the simulation and evolution of Antarctic ozone. *Geophysical Research Letters*, *43*, 9869–9876. https://doi.org/10.1002/2016GL070471

Oman, L. D., Douglass, A. R., Ziemke, J. R., Rodriguez, J. M., Waugh, D. W., & Nielsen, J. E. (2013). The ozone response to enso in aura satellite measurements and a chemistry-climate simulation. *Journal of Geophysical Research Atmospheres*, *118*(2), 965–976. https://doi.org/10.1029/2012JD018546

Ordóñez, C., Lamarque, J. F., Tilmes, S., Kinnison, D. E., Atlas, E. L., Blake, D. R., … Saiz-Lopez, A. (2012). Bromine and iodine chemistry in a global chemistry-climate model: Description and evaluation of very short-lived oceanic sources. *Atmospheric Chemistry and Physics*, *12*(3), 1423–1447. https://doi.org/10.5194/acp-12-1423-2012

Pan, L. L., Atlas, E. L., Salawitch, R. J., Honomichl, S. B., Bresch, J. F., Randel, W. J., … Wolfe, G. (2017). The Convective Transport of Active Species in the Tropics (CONTRAST) Experiment. *Bulletin of the American Meteorological Society*, *98*(1), 106–128. https://doi.org/10.1175/BAMS-D-14-00272.1

Pan, L. L., Bowman, K. P., Shapiro, M., Randel, W. J., Gao, R. S., Campos, T., … Barnet, C. (2007). Chemical behavior of the tropopause observed during the Stratosphere-Troposphere Analyses of Regional Transport experiment. *Journal of Geophysical Research*, *112*(D18), D18110. https://doi.org/10.1029/2007JD008645

Pan, L. L., Randel, W. J., Gary, B. L., Mahoney, M. J., & Hintsa, E. J. (2004). Definitions and sharpness of the extratropical tropopause: A trace gas perspective. *Journal of Geophysical Research: Atmospheres*, *109*(D23), 1–11. https://doi.org/10.1029/2004JD004982

Parrella, J. P., Chance, K., Salawitch, R. J., Canty, T., Dorf, M., & Pfeilsticker, K. (2013). New retrieval of BrO from SCIAMACHY limb: An estimate of the stratospheric bromine loading during April 2008. *Atmospheric Measurement Techniques*, *6*(10), 2549–2561. https://doi.org/10.5194/amt-6-2549-2013

Pfeilsticker, K., Sturges, W. T., Bösch, H., Camy-Peyret, C., Chipperfield, M. P., Engel, A., … Sinnhuber, B.-M. (2000). Lower Stratospheric Organic and Inorganic Bromine Budget for the Arctic Winter 1998/99. *Geophysical Research Letters*, *27*(20), 3305–3308.

Pitari, G., Aquila, V., Kravitz, B., Robock, A., Watanabe, S., Cionni, I., … Tilmes, S. (2014). Stratospheric ozone response to sulfate geoengineering: Results from the Geoengineering Model Intercomparison Project (GeoMIP). *Journal of Geophysical Research: Atmospheres*, *119*(5), 2629–2653. https://doi.org/10.1002/2013JD020566

Plumb, R. A., & Ko, M. K. W. (1992). Interrelationships Between Mixing Ratios of Long-Lived Stratospheric Constituents. *J. Geophys. Res.*, *97*(D9), 10145–10156.

Prinn, R. G., Weiss, R. F., Fraser, P. J., Simmonds, P. G., Cunnold, D. M., Alyea, F. N., … McCulloch, A. (2000). A history of chemically and radiatively important gases in air deduced from ALE/GAGE/AGAGE. *Journal of Geophysical Research: Atmospheres*, *105*(D14), 17751–17792. https://doi.org/10.1029/2000JD900141

Pyle, J. A., Ashfold, M. J., Harris, N. R. P., Robinson, A. D., Warwick, N. J., Carver, G. D., … Ong, S. (2011). Bromoform in the tropical boundary layer of the Maritime Continent during OP3. *Atmospheric Chemistry and Physics*, *11*(2), 529–542. https://doi.org/10.5194/acp-11-529-2011

Quack, B., & Wallace, D. W. R. (2003). Air-sea flux of bromoform: Controls, rates, and implications. *Global Biogeochemical Cycles*, *17*(1). https://doi.org/10.1029/2002GB001890

Revell, L. E., Stenke, A., Luo, B., Kremser, S., Rozanov, E., Sukhodolov, T., & Peter, T. (2017).

Impacts of Mt Pinatubo volcanic aerosol on the tropical stratosphere in chemistry-climate model simulations using CCMI and CMIP6 stratospheric aerosol data. *Atmospheric Chemistry and Physics*, *17*(21), 13139–13150. https://doi.org/10.5194/acp-17-13139-2017

Rex, M., Wohltmann, I., Ridder, T., Lehmann, R., Rosenlof, K., Wennberg, P., … Tegtmeier, S. (2014). A tropical West Pacific OH minimum and implications for stratospheric composition. *Atmospheric Chemistry and Physics*, *14*(9), 4827–4841. https://doi.org/10.5194/acp-14-4827-2014

Ridley, B. A., & Grahek, F. E. (1990). A Small, Low Flow, High Sensitivity Reaction Vessel for NO Chemiluminescence Detectors. *Journal of Atmospheric and Oceanic Technology*, *7*(2), 307–311. https://doi.org/10.1175/1520-0426(1990)007<0307:ASLFHS>2.0.CO;2

Robinson, A. D., Harris, N. R. P., Ashfold, M. J., Gostlow, B., Warwick, N. J., O'Brien, L. M., … Pyle, J. A. (2014). Long-term halocarbon observations from a coastal and an inland site in Sabah, Malaysian Borneo. *Atmospheric Chemistry and Physics*, *14*(16), 8369–8388. https://doi.org/10.5194/acp-14-8369-2014

Saiz-Lopez, A., Fernandez, R. P., Ordóñez, C., Kinnison, D. E., Martín, J. C. G., Lamarque, J. F., & Tilmes, S. (2014). Iodine chemistry in the troposphere and its effect on ozone. *Atmospheric Chemistry and Physics*, *14*(23), 13119–13143. https://doi.org/10.5194/acp-14-13119-2014

Sala, S., Bönisch, H., Keber, T., Oram, D. E., Mills, G., & Engel, A. (2014). Deriving an atmospheric budget of total organic bromine using airborne in situ measurements from the western Pacific area during SHIVA. *Atmospheric Chemistry and Physics*, *14*(13), 6903–6923. https://doi.org/10.5194/acp-14-6903-2014

Salawitch, R. J., Canty, T., Kurosu, T., Chance, K., Liang, Q., Da Silva, A., … Jacob, D. J. (2010). A new interpretation of total column BrO during Arctic spring. *Geophysical Research Letters*, *37*(21), 1–9. https://doi.org/10.1029/2010GL043798

Salawitch, R. J., Weisenstein, D. K., Kovalenko, L. J., Sioris, C. E., Wennberg, P. O., Chance, K., … McLinden, C. A. (2005). Sensitivity of ozone to bromine in the lower stratosphere. *Geophysical Research Letters*, *32*(5), 1–5. https://doi.org/10.1029/2004GL021504

Schauffler, S. M., Atlas, E. L., Blake, D. R., Flocke, F., Lueb, R. A., Lee-Taylor, J. M., … Travnicek, W. (1999). Distributions of brominated organic compounds in the troposphere and lower stratosphere. *Journal of Geophysical Research: Atmospheres*, *104*(D17), 21513–21535. https://doi.org/10.1029/1999JD900197

Schauffler, S. M., Atlas, E. L., Donnelly, S. G., Andrews, A., Montzka, S. A., Elkins, J. W., … Stroud, V. (2003). Chlorine budget and partitioning during the Stratospheric Aerosol and Gas Experiment (SAGE) III Ozone Loss and Validation Experiment (SOLVE). *Journal of Geophysical Research*, *108*(D5), 4173. https://doi.org/10.1029/2001JD002040

Schmidt, J. A., Jacob, D. J., Horowitz, H. M., Hu, L., Sherwen, T., Evans, M. J., … Volkamer, R. (2016). Modeling the observed tropospheric BrO background: Importance of multiphase chemistry and implications for ozone, OH, and mercury. *Journal of Geophysical Research: Atmospheres*, *121*(19), 11,819-11,835. https://doi.org/10.1002/2015JD024229

Schofield, R., Fueglistaler, S., Wohltmann, I., & Rex, M. (2011). Sensitivity of stratospheric Br_y to uncertainties in very short lived substance emissions and atmospheric transport. *Atmospheric Chemistry and Physics*, *11*(4), 1379–1392. https://doi.org/10.5194/acp-11-1379-2011

Schofield, R., Kreher, K., Conner, B. J., Johnston, P. V., Thomas, A., Shooter, D., … Mount, G. H. (2004). Retrieved tropospheric and stratospheric BrO columns over Lauder, New

Zealand. *Journal of Geophysical Research*, *109*(D14), D14304. https://doi.org/10.1029/2003JD004463

Scinocca, J. F., McFarlane, N. A., Lazare, M., Li, J., & Plummer, D. (2008). Technical Note: The CCCma third generation AGCM and its extension into the middle atmosphere. *Atmospheric Chemistry and Physics*, *8*(23), 7055–7074. https://doi.org/10.5194/acp-8-7055-2008

Shetter, R. E., & Müller, M. (1999). Photolysis frequency measurements using actinic flux spectroradiometry during the PEM-Tropics mission: Instrumentation description and some results. *Journal of Geophysical Research: Atmospheres*, *104*(D5), 5647–5661. https://doi.org/10.1029/98JD01381

Sinnhuber, B.-M., & Folkins, I. (2006). Estimating the contribution of bromoform to stratospheric bromine and its relation to dehydration in the tropical tropopause layer. *Atmospheric Chemistry and Physics*, *6*(12), 4755–4761. https://doi.org/10.5194/acp-6-4755-2006

Sinnhuber, B. M., & Meul, S. (2015). Simulating the impact of emissions of brominated very short lived substances on past stratospheric ozone trends. *Geophysical Research Letters*, *42*(7), 2449–2456. https://doi.org/10.1002/2014GL062975

Sioris, C. E., Kovalenko, L. J., McLinden, C. A., Salawitch, R. J., Van Roozendael, M., Goutail, F., … Frerick, J. (2006). Latitudinal and vertical distribution of bromine monoxide in the lower stratosphere from Scanning Imaging Absorption Spectrometer for Atmospheric Chartography limb scattering measurements. *Journal of Geophysical Research Atmospheres*, *111*(14), 1–25. https://doi.org/10.1029/2005JD006479

Solomon, S., Kinnison, D., Bandoro, J., & Garcia, R. (2015). Simulation of polar ozone depletion: An update. *Journal of Geophysical Research: Atmospheres*, *120*(15), 7958–7974. https://doi.org/10.1002/2015JD023365

SPARC. (2013). *SPARC Report on Lifetimes of Stratospheric Ozone-Depleting Substances, Their Replacements, and Related Species* (WCRP-15/20). (M. Ko, P. Newman, S. Reimann, & S. Strahan, Eds.), *SPARC Report* (Vol. No. 6). Retrieved from http://www.sparc-climate.org/publications/sparc-reports/

Stachnik, R. A., Millán, L., Jarnot, R., Monroe, R., McLinden, C., Kühl, S., … Pfeilsticker, K. (2013). Stratospheric BrO abundance measured by a balloon-borne submillimeterwave radiometer. *Atmospheric Chemistry and Physics*, *13*(6), 3307–3319. https://doi.org/10.5194/acp-13-3307-2013

Stenke, A., Schraner, M., Rozanov, E., Egorova, T., Luo, B., & Peter, T. (2013). The SOCOL version 3.0 chemistry-climate model: Description, evaluation, and implications from an advanced transport algorithm. *Geoscientific Model Development*, *6*(5), 1407–1427. https://doi.org/10.5194/gmd-6-1407-2013

Stone, K. A., Morgenstern, O., Karoly, D. J., Klekociuk, A. R., French, W. J., Abraham, N. L., & Schofield, R. (2016). Evaluation of the ACCESS - Chemistry-climate model for the Southern Hemisphere. *Atmospheric Chemistry and Physics*, *16*(4), 2401–2415. https://doi.org/10.5194/acp-16-2401-2016

Stutz, J., Werner, B., Spolaor, M., Scalone, L., Festa, J., Tsai, C., … Pfeilsticker, K. (2017). A new Differential Optical Absorption Spectroscopy instrument to study atmospheric chemistry from a high-altitude unmanned aircraft. *Atmospheric Measurement Techniques*, *10*(3), 1017–1042. https://doi.org/10.5194/amt-10-1017-2017

Tegtmeier, S., Krüger, K., Quack, B., Atlas, E. L., Pisso, I., Stohl, A., & Yang, X. (2012).

Emission and transport of bromocarbons: From the West Pacific ocean into the stratosphere. *Atmospheric Chemistry and Physics*, *12*(22), 10633–10648. https://doi.org/10.5194/acp-12-10633-2012

Theys, N., Van Roozendael, M., Hendrick, F., Fayt, C., Hermans, C., Baray, J.-L., … De Mazière, M. (2007). Retrieval of stratospheric and tropospheric BrO columns from multi-axis DOAS measurements at Reunion Island (21° S, 56° E). *Atmospheric Chemistry and Physics Discussions*, *7*(3), 8261–8308. https://doi.org/10.5194/acpd-7-8261-2007

Theys, N., Van Roozendael, M., Hendrick, F., Yang, X., De Smedt, I., Richter, A., … De Mazière, M. (2011). Global observations of tropospheric BrO columns using GOME-2 satellite data. *Atmospheric Chemistry and Physics*, *11*(4), 1791–1811. https://doi.org/10.5194/acp-11-1791-2011

Tian, W., & Chipperfield, M. P. (2005). A new coupled chemistry–climate model for the stratosphere: The importance of coupling for future O_3-climate predictions. *Quarterly Journal of the Royal Meteorological Society*, *131*(605), 281–303. https://doi.org/10.1256/qj.04.05

Tilmes, S., Kinnison, D. E., Garcia, R. R., Salawitch, R., Canty, T., Lee-Taylor, J., … Chance, K. (2012). Impact of very short-lived halogens on stratospheric ozone abundance and UV radiation in a geo-engineered atmosphere. *Atmospheric Chemistry and Physics*, *12*, 10945–10955. https://doi.org/10.5194/acp-12-10945-2012

Tilmes, S., Lamarque, J.-F., Emmons, L. K., Kinnison, D. E., Ma, P.-L., Liu, X., … Val Martin, M. (2015). Description and evaluation of tropospheric chemistry and aerosols in the Community Earth System Model (CESM1.2). *Geoscientific Model Development*, *8*(5), 1395–1426. https://doi.org/10.5194/gmd-8-1395-2015

Tilmes, S., Lamarque, J. F., Emmons, L. K., Kinnison, D. E., Marsh, D., Garcia, R. R., … Blake, N. (2016). Representation of the Community Earth System Model (CESM1) CAM4-chem within the Chemistry-Climate Model Initiative (CCMI). *Geoscientific Model Development*, *9*(5), 1853–1890. https://doi.org/10.5194/gmd-9-1853-2016

Tilmes, S., Muller, R., & Salawitch, R. (2008). The Sensitivity of Polar Ozone Depletion to Proposed Geoengineering Schemes. *Science*, *320*(5880), 1201–1204. https://doi.org/10.1126/science.1153966

Tokarczyk, R., & Moore, R. M. (1994). Production of volatile organohalogens by phytoplankton cultures. *Geophysical Research Letters*, *21*(4), 285–288. https://doi.org/10.1029/94GL00009

Voldoire, A., Sanchez-Gomez, E., Salas y Mélia, D., Decharme, B., Cassou, C., Sénési, S., … Chauvin, F. (2012). The CNRM-CM5.1 global climate model: description and basic evaluation. *Climate Dynamics*, *40*(9–10), 2091–2121. https://doi.org/10.1007/s00382-011-1259-y

Volk, C. M., Elkins, J. W., Fahey, D. W., Salawitch, R. J., Dutton, G. S., Gilligan, J. M., … Chan, K. R. (1996). Quantifying Transport Between the Tropical and Mid-Latitude Lower Stratosphere. *Science*, *272*(5269), 1763–1768. https://doi.org/10.1126/science.272.5269.1763

Volkamer, R., Baidar, S., Campos, T. L., Coburn, S., DiGangi, J. P., Dix, B., … Romashkin, P. A. (2015). Aircraft measurements of BrO, IO, glyoxal, NO_2, H_2O, O_2–O_2 and aerosol extinction profiles in the tropics: comparison with aircraft-/ship-based in situe and lidar measurements. *Atmospheric Measurement Techniques*, *8*(5), 2121–2148. https://doi.org/10.5194/amt-8-2121-2015

Wamsley, P. R., Elkins, J. W., Fahey, D. W., Dutton, G. S., Volk, C. M., Myers, R. C., … Salawitch, R. J. (1998). Distribution of halon-1211 in the upper troposphere and lower stratosphere and the 1994 total bromine budget. *Journal of Geophysical Research: Atmospheres*, *103*(D1), 1513–1526. https://doi.org/10.1029/97JD02466

Wang, S., Schmidt, J. A., Baidar, S., Coburn, S., Dix, B., Koenig, T. K., … Volkamer, R. (2015). Active and widespread halogen chemistry in the tropical and subtropical free troposphere. *Proceedings of the National Academy of Sciences*, *112*(30), 9281–9286. https://doi.org/10.1073/pnas.1505142112

Warwick, N. J., Pyle, J. A., Carver, G. D., Yang, X., Savage, N. H., O'Connor, F. M., & Cox, R. A. (2006). Global modeling of biogenic bromocarbons. *Journal of Geophysical Research Atmospheres*, *111*(24), 1–12. https://doi.org/10.1029/2006JD007264

Werner, B., Stutz, J., Spolaor, M., Scalone, L., Raecke, R., Festa, J., … Pfeilsticker, K. (2017). Probing the subtropical lowermost stratosphere and the tropical upper troposphere and tropopause layer for inorganic bromine. *Atmospheric Chemistry and Physics*, *17*(2), 1161–1186. https://doi.org/10.5194/acp-17-1161-2017

Wisher, A., Oram, D. E., Laube, J. C., Mills, G. P., Van Velthoven, P., Zahn, A., & Brenninkmeijer, C. A. M. (2014). Very short-lived bromomethanes measured by the CARIBIC observatory over the North Atlantic, Africa and Southeast Asia during 2009-2013. *Atmospheric Chemistry and Physics*, *14*(7), 3557–3570. https://doi.org/10.5194/acp-14-3557-2014

Wofsy, S. C., McElroy, M. B., & Yung, Y. L. (1975). The chemistry of atmospheric bromine. *Geophysical Research Letters*, *2*(6), 215–218. https://doi.org/10.1029/GL002i006p00215

World Meteorological Organization. (1957). Meteorology—A three-dimensional science: Second session of the Commission for Aerology. *WMO Bull.*

Yang, X., Cox, R. A., Warwick, N. J., Pyle, J. A., Carver, G. D., O'Connor, F. M., & Savage, N. H. (2005). Tropospheric bromine chemistry and its impacts on ozone: A model study. *Journal of Geophysical Research Atmospheres*, *110*(23), 1–18. https://doi.org/10.1029/2005JD006244

Yukimoto, S., Adachi, Y., Hosaka, M., Sakami, T., Yoshimura, H., Hirabara, M., … Kitoh, A. (2012). A New Global Climate Model of the Meteorological Research Institute: MRI-CGCM. *Journal of the Meteorological Society of Japan*, *90A*(0), 23–64. https://doi.org/10.2151/jmsj.2012-A02

Ziska, F., Quack, B., Abrahamsson, K., Archer, S. D., Atlas, E., Bell, T., … Yokouchi, Y. (2013). Global sea-to-air flux climatology for bromoform, dibromomethane and methyl iodide. *Atmospheric Chemistry and Physics*, *13*(17), 8915–8934. https://doi.org/10.5194/acp-13-8915-2013

Zondlo, M. A., Paige, M. E., Massick, S. M., & Silver, J. A. (2010). Vertical cavity laser hygrometer for the National Science Foundation Gulfstream-V aircraft. *Journal of Geophysical Research*, *115*(D20), D20309. https://doi.org/10.1029/2010JD014445